A NEW HIERARCHICAL METHOD FOR IMAGE SEGMENTATION AND INPAINTING USING MUMFORD-SHAH MODEL

XIAOJUN DU

A THESIS

IN

THE DEPARTMENT

OF

COMPUTER SCIENCE AND SOFTWARE ENGINEERING

PRESENTED IN PARTIAL FULFILLMENT OF THE REQUIREMENTS

FOR THE DEGREE OF MASTER OF COMPUTER SCIENCE

CONCORDIA UNIVERSITY

MONTRÉAL, QUÉBEC, CANADA

APRIL 2006

Your file Votre référence
ISBN: 978-0-494-20775-8
Our file Notre référence
ISBN: 978-0-494-20775-8

Abstract

A New Hierarchical Method for Image Segmentation and Inpainting Using Mumford-Shah Model

XIAOJUN DU

Image segmentation is a popular topic in computer vision and image processing. As a region-based (global) approach, the Mumford and Shah (MS) model is a powerful and robust segmentation technique as compared to edge-based (local) methods. However, there are some difficulties with the MS model. One difficulty is the detection of roof edges. In this thesis, we first modify the MS model to include second order derivative term and use linear approximation to implement the solution. In this way, we can detect not only step edges but also creases and roof edges. The most important difficulty of MS model is that the segmentation results depend on the initial curves. To overcome this problem, we present in this thesis a hierarchical strategy that takes into account both the local information at the pixel level and the global information of the MS model. With this hierarchical segmentation scheme, we can segment an image into regions until each region is smooth enough and need no additional segmentation. Compared with previous works, our approach can automatically detect both main structure and details in an image with multi-level-set functions, and it can stop automatically when the boundaries are detected. In our approach, the final segmentation does not depend on the initial condition. Many experimental results indicate that our approach is effective in many applications. Especially, we apply the new approach to the image inpainting problem. Compared with previous work, because the new approach can detect all the edges in an image, it can preserve more edges and details in the inpainting process.

Acknowledgments

I would like to express my sincere gratitude to my advisor Professor Tien D. Bui for his guidance, help and support. His advice gave me much inspiration for the thesis work.

I thank my fellow students Song Gao and Qinghui Zhang for their wonderful previous works. I would also like to thank Dongwook Cho and other members of the Professor Bui's group for useful discussions.

I thank my wife for her support and encouragement.

Contents

List of Figures

Chapter 1

Introduction

Image segmentation is a popular topic in computer vision and image processing. Because it is widely used in image analysis, image registration, image compression, reconstruction, inpainting, enhancement and denoise, the technique of image segmentation has received much attention.

Because researchers have different interests in different applications, it is difficult to propose a common definition of image segmentation. In this thesis, we define image segmentation as partitioning an image into different regions, so that the image intensity is smooth inside each region and changes abruptly on the boundaries of these regions.

The variational approach is an important technique for image segmentation. In this technique, we try to minimize an energy to segment an image. This technique can be divided into two categories: edge-based and region-based approaches. The snake model is an edge-based variational approach [42, 33]. The final segmentation contour corresponds to the minimum of following energy:

$$J(C) = \int_0^1 \alpha(s)|C'(s)|^2 ds + \int_0^1 \beta(s)|C''(s)|^2 ds + \lambda \int_0^1 g^2(|\nabla u(C(s))|) ds \quad (1)$$

where s is a point on the segmentation contour $C(s)$. The first two terms represent the internal energy and control the deformation of the contour. There are two non-negative parameter functions: $\alpha(s)$ controls the tension of the contour while $\beta(s)$ controls its rigidity. The last term is the external energy and attracts the contour toward the intensity edges within an image. There are two drawbacks

of the this approach: the result depends on the parameters α and β, and this model cannot handle changes in the topology of the evolving contour directly. In fact, it is impossible to detect more than one object simultaneously [20].

If we set the rigidity term to zero that is $\beta = 0$, the energy becomes:

$$J_1(C) = \int_0^1 \alpha(s)|C'(s)|^2 ds + \lambda \int_0^1 g^2(|\nabla u(C(s))|) ds \tag{2}$$

[7, 34] presented the following energy functional:

$$J_2(C) = 2\sqrt{\lambda} \int_0^1 g(|\nabla u(C(s))|)|C'(s)| ds \tag{3}$$

and [35] proved that minimizing the energy functional $J_2(C)$ is equivalent to minimizing $J_1(C)$. $J_2(C)$ is called geodesic active contours model. This model is intrinsic because it does not depend on the parameterization of the curve. In addition, [20] proposed that $J_2(C)$ can be solved by using the level set methods.

The level set method is first introduced by Osher and Sethian [22, 24, 25, 26, 27, 28]. It is a numerical technique to analyze and compute the motion of interface. The technique can handle changes in topology of the evolving curve and is fast.

Both the snakes model and the geodesic active contours model only use edge detector function (∇u_0) to stop the evolving curve on the edges of the object. Therefore they belong to the edge-based approach.

On the other hand, the region-based approaches make use of the information not only near the boundary of objects but also inside the object regions. Mumford-Shah (MS) model [3] belongs to this category. In this model, we try to find an optimal piecewise smooth approximation u of the original image u_0, and a set of boundaries C, such that u varies smoothly inside the homogeneous regions and discontinuously or rapidly across C. Compared with edge-based approaches, MS model is more robust and can deal with noisy images. However, the numerical method of solving the MS model is difficult to implement. There are some alternative solutions to this problem. Some researchers used elliptic approximation to form weak formulation of MS model [20, 36, 37, 38]. Another kind of

approaches are based on level set technique. This category includes the active contours without edges model [4], the multiphase level set framework [5], the curve evolution based approach [1], the image segmentation and selective smoothing [2], and etc.. The piecewise constant approximation presented by Chan and Vese is one example [4]. The authors approximate the intensity inside each segmented region in an image by a constant gray value. Compared with the piecewise smooth approximation approach in [5], the piecewise constant approximation approach only solve one partial differential equation (PDE) instead of three coupled PDEs. It is faster and more robust.

While MS model works well in many applications, it also faces some difficulties:

1. The piecewise constant approximation is suitable only to the situation in which the intensities of the segmented regions in an image are uniform.

2. While the MS model can detect step edges, roof edges are often missed.

3. When the level set method is implemented to solve the curve evolution, 2^n regions can be represented by n level set functions. It is supposed that any number of regions can be segmented as long as enough level set functions are used. However, this is not true. Besides the high computational cost to solve coupled multi level set functions, the results of curve evolution depend on the initial location of the level sets. Because the MS energy functional is not convex, the minimization of the functional is often trapped by a local minimum. Consequently, in most cases, it is difficult for the initial curves to evolve to the proper boundaries of objects in an image.

To overcome the first difficulty, Zhang [29] presents a piecewise linear approximation for MS model to adapt to the image intensities distribution inside segmented regions. He also generalizes the MS model to detect low contrast edges and roof edges. In this thesis, we propose to use second derivative term to detect roof edges.

For the third difficulty, we present a new hierarchical segmentation scheme to obtain better segmentation results compared to many previous methods. Our approach is different from previous hierarchical segmentation approaches proposed in [1] and [2] . In this thesis, we combine the global

approach of the MS model with the local information at the pixel level. With this scheme, we can detect both large objects as well as small and detailed structures. It is believed that our approach can be used for complicated images. The most important advantage is that the segmentation result does not depend on the initial conditions.

The organization of the thesis is as following: First, the MS model and Level set technique are introduced in chapter two; the piecewise smooth and piecewise constant approximations are reviewed in chapter three. The piecewise linear approximation and modified MS model are presented in chapter four. In chapter five, we present the new hierarchical segmentation scheme, and experimental results are presented in chapter six. In chapter seven, an application of our hierarchical image segmentation scheme in image inpainting is presented. Finally the conclusion is reached in chapter eight.

Chapter 2

The Mumford-Shah Model and the Level Set Approach

In this chapter, we will review the Mumford-Shah model and the level set method in the context of the image segmentation problem.

2.1 Image Segmentation

The problem of image segmentation can be defined as follows: For an observed image u_0 (possibly with noise), we want to find an optimal piecewise smooth approximation u of u_0 for each specific region. The regions are denoted by Ω_i, $i = 1, 2, ..., n$. The function u varies smoothly within Ω_i, and rapidly or discontinuously across the boundaries of Ω_i. The boundaries of all Ω_i are denoted as C. The whole image can be expressed as:

$$\Omega = \bigcup \Omega_i \bigcup C. \tag{4}$$

The process to find the boundaries of Ω_i is called segmentation. Mumford and Shah proposed that the segmentation of an image can be obtained through the minimization of a energy functional

known as the Mumford-Shah energy functional [3]:

$$E(u,C) = \int_{\Omega\setminus C} |u-u_0|^2 dxdy + \mu \int_{\Omega\setminus C} |\nabla u|^2 dxdy + \nu|C|, \quad (5)$$

In equation (5), u_0 is the original image; u is the smooth approximation of the image; C is the segmentation curve; $|C|$ represents the length of the curve; Ω is the image domain; Ω/C represents the image domain excluding the segmentation curve. If the MS energy functional is minimized, the image will be segmented into regions so that: (1) u is a good approximation of u_0, (2) u is smooth in each region, and (3) the boundary of each region is as short as possible. The parameters of μ and ν are used to balance the affects of different terms.

2.2 Markov Random Field Model

The Mumford-Shah (MS) model can be understood in the following way: For an observed noisy image u_0, we would like to find the true (clean) image u. Using Bayesian decision theorem, the posterior probability is $P(u|u_0) = P(u_0|u)\ P(u)$. Here $P(u)$ is the probability of obtaining u, and $P(u_0|u)$ is the probability of obtaining u_0 given the image u. Then $P(u|u_0)$ is the probability of obtaining the (clean) segmentation image u given u_0.

We assume that $P(u)$ is proportional to the energy in the following form [12] $P(u) = \exp(-U)$. Here U is energy of the image. Considering only interactions between neighboring sites of the image, U can be expressed as

$$U \propto \sum_{i \text{ and } j \text{ are neighbor pixels}} g(u(i)-u(j)) \propto \sum g(\nabla u) \quad (6)$$

Where $g(x)$ is the regularization function; i and j are the indices of pixels in the image. $P(u_0|u)$ is assumed to be

$$\begin{aligned} P(u_0|u) &\propto \prod_{i=1}^{N} \exp[-(u_0(i)-u(i))^2] \\ &\propto \exp[-\int (u_0-u)^2 dx] \end{aligned} \quad (7)$$

Assuming $P(u|u_0) = \exp(-E(u,u_0))$, then we have

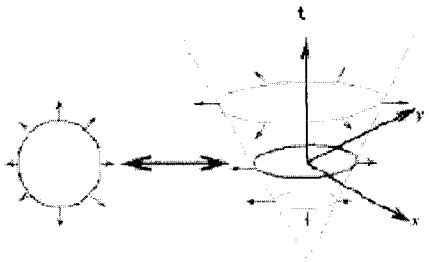

Figure 1: *The 3-dimension demonstration of level set approach [9].*

$$E(u) = \int (u - u_0)^2 dx + \mu \int g(\nabla u) dx \tag{8}$$

If we include the boundary energy in Eq.(8), we have

$$E(u, C) = \int (u - u_0)^2 dx + \mu \int g(\nabla u) dx + \nu |C| \tag{9}$$

When $g(x) = |x|^2$, (9) becomes the Mumford-Shah model.

The solution of the MS energy functional is not a trivial task. There are some alternative solutions to this problem, such as the elliptic approximation to the weak formulation of the MS functional [20], the active contours without edges [4, 5], and the hierarchical curve evolution based approaches in [1, 2].

2.3 Level Set Approach

The level set method is first introduced by Osher and Sethian [22, 24, 25, 26, 27, 28]. It is a numerical technique to analyze and compute the motion of interfaces. Many applications of the level set method are developed in image processing.

The basic idea of the level set method is to make use of a 3-dimension surface to represent the motion of a 2-dimension curve as shown in figure 1.

In figure 1, the 3-dimension cone-shaped surface represents the motion of a 2-dimension circle curve. The intersection between the cone-shaped surface and the x-y plane represents the curve at different time. In this figure, the circle becomes bigger along the time axis. The 3-dimension surface can be represented by an equation $\phi(x, y, z) = 0$. This surface segments the plane into two regions,

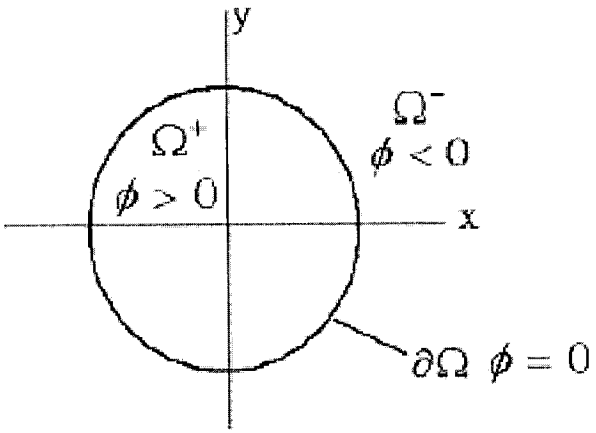

Figure 2: *Representation of two regions by a level set function [30].*

inside region and outside region. We can assume $\phi(x, y, z) > 0$ inside the region and $\phi(x, y, z) < 0$ outside the region. On the x-y plane, the relationship becomes:

$$\phi(x, y, t) \begin{cases} > 0 \text{ inside the curve} \\ = 0 \text{ on the curve} \\ < 0 \text{ outside the curve} \end{cases} \tag{10}$$

As shown in figure 2, we can use the function $\phi(x, y, t)$, level set function, to represent two regions, inside region and outside region. We also can use two level set functions to represent four regions as shown in figure 3. The two level set functions satisfy:

$$\begin{aligned} &\phi_1 > 0, \phi_2 > 0 \text{ inside region 1} \\ &\phi_1 < 0, \phi_2 > 0 \text{ inside region 2} \\ &\phi_1 > 0, \phi_2 < 0 \text{ inside region 3} \\ &\phi_1 < 0, \phi_2 < 0 \text{ inside region 4} \end{aligned} \tag{11}$$

In this way, we can use n level set functions to represent 2^n regions.

As mentioned in the beginning, the motion of a curve can be represented by a 3-dimension surface. Since the surface is represented by equation: $\phi(x, y, t) = 0$, at any time t the level set value

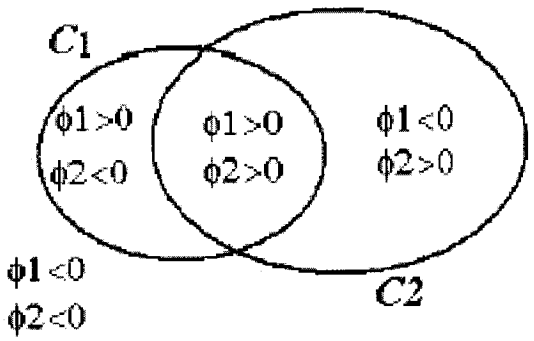

Figure 3: *Representation of four regions by two level set functions [5].*

of each point $x(\vec{t})$ on the surface is always zero. This implies $d\phi(x(\vec{t}),t)/dt = 0$. By the chain rule we have:

$$\frac{\partial\phi(\vec{x},t)}{\partial t} + \nabla\phi \cdot \frac{d\vec{x}}{dt} = 0 \tag{12}$$

It is an initial value partial differential equation and can be written as:

$$\frac{\partial\phi(\vec{x},t)}{\partial t} + F|\nabla\phi| = 0 \tag{13}$$

We also need two conditions for the equation:

1. The boundary condition: we usually impose the normal derivative vanishes on the curve or the surface.

$$\frac{\partial\phi}{\partial\vec{n}} = 0 \text{ on the curve} \tag{14}$$

where $\vec{n}$ is the normal vector.

2. The initial condition: The initial function $\phi_0(x,y)$ usually is assumed to be an initial curve.

$$\phi(x,y,0) = \phi_0(x,y) \tag{15}$$

By solving equation (13), we can obtain the evolution of a 2-dimension curve.

An example of the evolution of a curve is to assume $F = -\kappa$, where κ is the curvature of the

curve. In this case, the motion equation becomes:

$$\frac{\partial \phi(\vec{x},t)}{\partial t} = \nabla \left(\frac{\nabla \phi}{|\nabla \phi|} \right) |\nabla \phi| \tag{16}$$

If we assume a square initial curve, the evolution of the curve is shown in figure 4. In figure 4, the

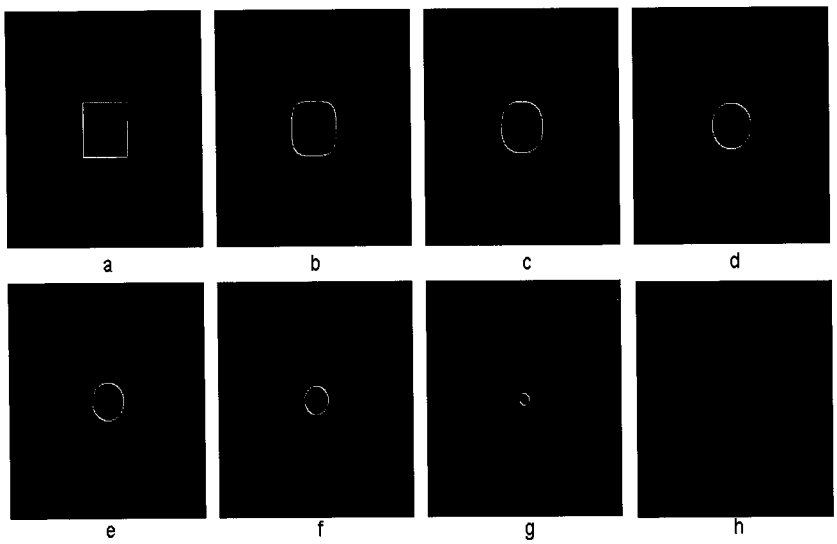

Figure 4: *The evolution of a square curve.*

square curve first evolves to a circle and then vanishes.

There are many advantages to use the level set method to solve the evolution of curves, including:

1. The topological changes in the evolving boundary such as merging and breaking are handled naturally as shown in figure 5.

2. The numerical solution of the motion equation is easy to implement.

The formulation of the MS model leads itself to the level set method as a numerical approach for solving the MS energy functional, in which the contour C can be presented by the level set function ϕ. This concept will be made clear in the following chapters.

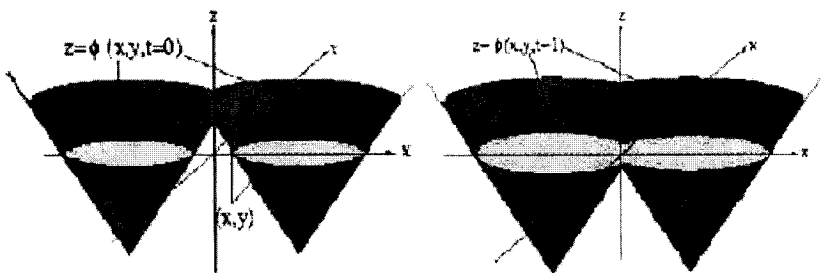

Figure 5: *The merge of two curves with level-set approach [9].*

Chapter 3

Piecewise Smooth and Piecewise Constant Approximations of Mumford-Shah Model

The solution of the MS energy functional is not a trivial task. There are some alternative solutions to this problem, such as the elliptic approximation to the weak formulation of the MS functional [20], the active contours without edges [4, 5], and the hierarchical curve evolution based approaches in [1, 2]. Because the work of this thesis is mainly based on and extended from the two approaches: piecewise smooth and piecewise constant approximations of the MS model, these two approaches are introduced in the following sections.

3.1 Piecewise Smooth Approximation

If we consider that a closed curve segments an image into two regions (i.e. inside and outside regions), the MS energy functional can be written as:

$$\begin{aligned} E(u_1, u_2, C) &= \int_{\text{inside } C} |u_1 - u_0|^2 \, dxdy + \mu \int_{\text{inside } C} |\nabla u_1|^2 \, dxdy \\ &+ \int_{\text{outside } C} |u_2 - u_0|^2 \, dxdy + \mu \int_{\text{outside } C} |\nabla u_2|^2 \, dxdy + \nu \cdot |C|, \end{aligned} \tag{17}$$

where u_1 and u_2 are smooth approximations of the image inside and outside the curve. The numerical solution of the MS energy functional can be implemented by the level set method. In the case that the image consists of two regions, the segmentation curve can be represented by one level set function ϕ:

$$\phi(x, y, t) = \begin{cases} > 0 & \text{if } (x, y) \text{ is inside } C \\ = 0 & \text{if } (x, y) \text{ is on } C \\ < 0 & \text{if } (x, y) \text{ is outside } C \end{cases} \tag{18}$$

Using the level set functions and the Heaviside function $H(x)$ defined by

$$H(x) = \begin{cases} 1 \text{ if } x > 0 \\ 0 \text{ if } x < 0 \end{cases} \tag{19}$$

the piecewise smooth approximation of the MS model can be written as:

$$\begin{aligned} E(u_1, u_2, \phi) &= \int (u_1 - u_0)^2 H(\phi) dxdy + \int (u_2 - u_0)^2 (1 - H(\phi)) dxdy \\ &+ \mu \int |\nabla u_1|^2 H(\phi) dxdy + \mu \int |\nabla u_2|^2 (1 - H(\phi)) dxdy \\ &+ \nu \int |\nabla H(\phi)| dxdy. \end{aligned} \tag{20}$$

The numerical form of $H(x)$ is:

$$H_\epsilon(x) = \frac{1}{2}(1 + \frac{2}{\pi} \arctan(\frac{x}{\epsilon})) \tag{21}$$

Using the formula:

$$\nabla H(\phi) = \delta(\phi) \nabla \phi \tag{22}$$

where $\delta(\phi)$ is the Dirac function, we have:

$$\begin{aligned} E(u_1,u_2,\phi) &= \int (u_1-u_0)^2 H(\phi)dxdy + \int (u_2-u_0)^2(1-H(\phi))dxdy \\ &+\mu\int |\nabla u_1|^2 H(\phi)dxdy + \mu\int |\nabla u_2|^2 (1-H(\phi))dxdy \\ &+\nu\int \delta(\phi)|\nabla\phi|dxdy. \end{aligned} \tag{23}$$

The numerical form of $\delta(x)$ is:

$$\delta_\epsilon(x) = \frac{1}{\pi}\frac{\epsilon}{x^2+\epsilon^2} \tag{24}$$

We define:

$$\begin{aligned} F(u_1,u_2,\phi) &= (u_1-u_0)^2 H(\phi) + (u_2-u_0)^2(1-H(\phi)) \\ &+\mu|\nabla u_1|^2 H(\phi) + \mu|\nabla u_2|^2(1-H(\phi)) + \nu[\delta(\phi)|\nabla\phi|] \end{aligned} \tag{25}$$

Following the derivation of the Euler-Lagrange equation, we have

$$\begin{aligned} \frac{\partial F}{\partial\phi} &= (u_1-u_0)^2\delta(\phi) - (u_2-u_0)^2\delta(\phi) \\ &+\mu|\nabla u_1|^2\delta(\phi) - \mu|\nabla u_2|^2\delta(\phi) + \nu[\delta'(\phi)|\nabla\phi|] \end{aligned} \tag{26}$$

and

$$\frac{\partial}{\partial y}(\frac{\partial F}{\partial\phi_x}) = \nu[\delta'(\phi)\frac{\phi_x^2}{\sqrt{\phi_x^2+\phi_y^2}} + \delta(\phi)\frac{\partial}{\partial x}\frac{\phi_x}{\sqrt{\phi_x^2+\phi_y^2}}] \tag{27}$$

and

$$\frac{\partial}{\partial y}(\frac{\partial F}{\partial\phi_y}) = \nu[\delta'(\phi)\frac{\phi_y^2}{\sqrt{\phi_x^2+\phi_y^2}} + \delta(\phi)\frac{\partial}{\partial y}\frac{\phi_y}{\sqrt{\phi_x^2+\phi_y^2}}] \tag{28}$$

Thus, we have the following Euler-Lagrange equation:

$$\delta(\phi)[(u_1-u_0)^2 - (u_2-u_0)^2 + \mu|\nabla u_1|^2 - \mu|\nabla u_2|^2 - \nu\nabla\cdot(\frac{\nabla\phi}{|\nabla\phi|})] = 0 \tag{29}$$

with the boundary condition

$$\frac{\delta(\phi)}{|\nabla\phi|}\nabla\phi\cdot\hat{n} = \frac{\delta(\phi)}{|\nabla\phi|}\frac{\partial\phi}{\partial n} = 0. \tag{30}$$

Here $\hat{n}$ is the normalized normal of the boundary curve of the image. Using the gradient projection method, we can change equation (29) to the following time dependent equation

$$\frac{\partial \phi}{\partial t} = \delta(\phi)[-(u_1 - u_0)^2 + (u_2 - u_0)^2 - \mu \left|\nabla u_1\right|^2 + \mu \left|\nabla u_2\right|^2 + \nu \nabla \cdot (\frac{\nabla \phi}{|\nabla \phi|})]. \tag{31}$$

Similarly, we also can obtain the Euler-Lagrange equation for the variables of u_1, u_2:

$$\begin{aligned} (u_1 - u_0) &= \mu \nabla^2 u_1 \text{ inside } C \\ \frac{\partial u_1}{\partial \vec{n}} &= 0 \text{ on } C \end{aligned} \tag{32}$$

$$\begin{aligned} (u_2 - u_0) &= \mu \nabla^2 u_2 \text{ outside } C \\ \frac{\partial u_2}{\partial \vec{n}} &= 0 \text{ on } C \end{aligned} \tag{33}$$

The smooth image functions u_1 and u_2 can be obtained by solving the damped Poisson equations (32) and (33), and the segmentation curve can evolve according to equation (31). This is the piecewise smooth approximation presented by Chan and Vese [5]. Many advantages can be achieved by this approach, such as simultaneous segmentation and smoothing of noisy images, and detection of triple junctions by using multiple level set functions. However, because three PDEs equations (32), (33), and (31) are needed to be solved simultaneously, the computational cost of this approach is very large. To overcome this difficulty, Chan and Vese proposed another approach using the piecewise constant approximation [4, 5].

3.2 Piecewise Constant Approximation

If the image intensities inside different regions are uniform, the image intensities inside different regions can be approximated by constants. In this case, the MS energy functional can be simplified to equation (34):

$$E(c_k, C) = \sum_k \int_{\Omega_k} (c_k - u_0)^2 dxdy + \nu |C|, \tag{34}$$

where Ω_k represents the area inside each region. The gradient term in the MS energy functional disappears in equation (34) because the gradient inside each region is zero. Using the level set

method [9] and the MS energy functional of the two phase segmentation, the image is segmented into two regions:

$$\begin{aligned} E(c_1, c_2, \phi) &= \int (c_1 - u_0)^2 H(\phi) dxdy \\ &+ \int (c_2 - u_0)^2 (1 - H(\phi)) dxdy + \nu \int \delta(\phi) |\nabla \phi| dxdy \end{aligned} \tag{35}$$

where $H(x)$ is the Heaviside function.

We define:

$$F(\phi) = (c_1 - u_0)^2 H(\phi) + (c_2 - u_0)^2 (1 - H(\phi)) + \nu[\delta(\phi)|\nabla \phi|] \tag{36}$$

Following the derivation of the Euler-Lagrange equation, we have

$$\frac{\partial F}{\partial \phi} = (c_1 - u_0)^2 \delta(\phi) - (c_2 - u_0)^2 \delta(\phi) + \nu[\delta'(\phi)|\nabla \phi|] \tag{37}$$

and

$$\frac{\partial}{\partial y}(\frac{\partial F}{\partial \phi_x}) = \nu[\delta'(\phi) \frac{\phi_x^2}{\sqrt{\phi_x^2 + \phi_y^2}} + \delta(\phi) \frac{\partial}{\partial x} \frac{\phi_x}{\sqrt{\phi_x^2 + \phi_y^2}}] \tag{38}$$

and

$$\frac{\partial}{\partial y}(\frac{\partial F}{\partial \phi_y}) = \nu[\delta'(\phi) \frac{\phi_y^2}{\sqrt{\phi_x^2 + \phi_y^2}} + \delta(\phi) \frac{\partial}{\partial y} \frac{\phi_y}{\sqrt{\phi_x^2 + \phi_y^2}}] \tag{39}$$

Thus, we have the following Euler-Lagrange equation:

$$\delta(\phi)[(c_1 - u_0)^2 - (c_2 - u_0)^2 - \nu \nabla \cdot (\frac{\nabla \phi}{|\nabla \phi|})] = 0 \tag{40}$$

with the boundary condition

$$\frac{\delta(\phi)}{|\nabla \phi|} \nabla \phi \cdot \hat{n} = \frac{\delta(\phi)}{|\nabla \phi|} \frac{\partial \phi}{\partial n} = 0. \tag{41}$$

Here $\hat{n}$ is the normalized normal of the boundary curve of the image. Using the gradient projection method, we can change equation (40) to the following time dependent equation

$$\frac{\partial \phi}{\partial t} = \delta(\phi)[-(c_1 - u_0)^2 + (c_2 - u_0)^2 + \nu \nabla \cdot (\frac{\nabla \phi}{|\nabla \phi|})]. \tag{42}$$

equation (42) is the evolution function for the segmentation curve. Constants c_1 and c_2 can be solved by:

$$\frac{\partial E}{\partial c_1} = 0, \quad \frac{\partial E}{\partial c_2} = 0. \tag{43}$$

Thus

$$c_1(\phi) = \frac{\int u_0 H(\phi) dxdy}{\int H(\phi) dxdy} \tag{44}$$

$$c_2(\phi) = \frac{\int u_0 (1 - H(\phi)) dxdy}{\int (1 - H(\phi)) dxdy} \tag{45}$$

After solving these equations, we can obtain the information on c_1, c_2, and C. The image u_0 will then be segmented into two regions $\{u = c_1\}$ and $\{u = c_2\}$. Compared with the piecewise smooth approximation approach, the piecewise constant approximation approach is much faster because only one PDE needs to be solved. However, this approach is effective only when the intensity inside each segmented region (object) is uniform and can be approximated by a constant. When the intensities smoothly vary inside the object regions, the piecewise constant approximation will introduce bigger errors, and this approximation will not work well. Furthermore, in the case of roof edges, the variance of the intensities in the regions on both sides of the roof edge is large but the second order derivative is small, and the intensities inside these two regions cannot be approximated by constants. The bigger the variance inside the object regions, the bigger the error introduced by constant approximation. Therefore, the piecewise constant approximation will not detect roof edges correctly. To overcome this difficulty, Zhang in [29] presents the piecewise linear approximation approach. We can use a linear functional to approximate the intensity distribution in objects. This approach not only can keep the simplicity of the computation, i.e. we only solve one PDE, but also can adapt to the intensity variance of objects. In this way, we can obtain better segmentation results. For roof edges, we modify the MS energy functional and use linear approximation. Experimental results show that we can detect roof edges correctly.

If the image consists four regions, the segmentation curve can be represented by two level set functions ϕ_1 and ϕ_2, and the four regions are represented by the signs of the two level set functions:

Region 1: $\phi_1 > 0$ and $\phi_2 > 0$;

Region 2: $\phi_1 > 0$ and $\phi_2 < 0$;

Region 3: $\phi_1 < 0$ and $\phi_2 > 0$;

Region 4: $\phi_1 < 0$ and $\phi_2 < 0$.

With the piecewise constant approximation, the MS energy functional becomes:

$$\begin{aligned}
&E(c_{11}, c_{01}, c_{10}, c_{00}, \phi_1, \phi_2) = \\
&\int [(u_0 - c_{11})^2 H(\phi_1) H(\phi_2) + (u_0 - c_{10})^2 H(\phi_1)(1 - H(\phi_2)) \\
&+(u_0 - c_{01})^2 (1 - H(\phi_1)) H(\phi_2) + (u_0 - c_{00})^2 (1 - H(\phi_1))(1 - H(\phi_2))] dxdy \\
&+\nu \int |\nabla H(\phi_1)| dxdy + \nu \int |\nabla H(\phi_2)| dxdy
\end{aligned} \tag{46}$$

where c_{11}, c_{01}, c_{10}, and c_{00} are the average intensities in corresponding regions:

$$\begin{aligned}
c_{11} &= mean(u_0) \text{ in } \{\phi_1 > 0 \text{ and } \phi_2 > 0\} \\
c_{00} &= mean(u_0) \text{ in } \{\phi_1 < 0 \text{ and } \phi_2 < 0\} \\
c_{10} &= mean(u_0) \text{ in } \{\phi_1 > 0 \text{ and } \phi_2 < 0\} \\
c_{01} &= mean(u_0) \text{ in } \{\phi_1 < 0 \text{ and } \phi_2 > 0\}
\end{aligned} \tag{47}$$

We define

$$\begin{aligned}
F_4(\phi_1, \phi_2) \quad = \quad & (u_0 - c_{11})^2 H(\phi_1) H(\phi_2) + (u_0 - c_{10})^2 H(\phi_1)(1 - H(\phi_2)) \\
& +(u_0 - c_{01})^2 (1 - H(\phi_1)) H(\phi_2) + (u_0 - c_{00})^2 (1 - H(\phi_1))(1 - H(\phi_2)) \\
& +\nu |\nabla H(\phi_1)| + \nu |\nabla H(\phi_2)|
\end{aligned} \tag{48}$$

we have

$$\begin{aligned}
\frac{\partial F_4}{\partial \phi_1} \quad = \quad & (c_{11} - u_0)^2 \delta(\phi_1) H(\phi_2) + (c_{10} - u_0)^2 \delta(\phi_1)(1 - H(\phi_2)) \\
& -(c_{01} - u_0)^2 \delta(\phi_1) H(\phi_2) - (c_{00} - u_0)^2 \delta(\phi_1)(1 - H(\phi_2)) \\
& +\nu \delta'(\phi_1) |\nabla \phi_1|
\end{aligned} \tag{49}$$

and

$$\frac{\partial}{\partial x}(\frac{\partial F_4}{\partial \phi_{1x}}) = \nu[\delta'(\phi_1)\frac{\phi_{1x}^2}{\sqrt{\phi_{1x}^2+\phi_{1y}^2}} + \delta(\phi_1)\frac{\partial}{\partial x}\frac{\phi_{1x}}{\sqrt{\phi_{1x}^2+\phi_{1y}^2}}] \tag{50}$$

and

$$\frac{\partial}{\partial y}(\frac{\partial F_4}{\partial \phi_{1y}}) = \nu[\delta'(\phi_1)\frac{\phi_{1y}^2}{\sqrt{\phi_{1x}^2+\phi_{1y}^2}} + \delta(\phi_1)\frac{\partial}{\partial y}\frac{\phi_{1y}}{\sqrt{\phi_{1x}^2+\phi_{1y}^2}}] \tag{51}$$

Therefore, we have the following Euler-Lagrange equation for ϕ_1:

$$\begin{aligned}&\delta(\phi_1)\left[[(c_{11}-u_0)^2-(c_{01}-u_0)^2]H(\phi_2)+\right.\\&\left.[(c_{10}-u_0)^2-(c_{00}-u_0)^2](1-H(\phi_2))-\nu\nabla\cdot(\frac{\nabla\phi_1}{|\nabla\phi_1|})\right]=0\end{aligned} \tag{52}$$

with the boundary condition

$$\frac{\delta(\phi_1)}{|\nabla\phi_1|}\nabla\phi_1\cdot\hat{n}=\frac{\delta(\phi_1)}{|\nabla\phi_1|}\frac{\partial\phi_1}{\partial n}=0. \tag{53}$$

Here $\hat{n}$ is the normalized normal of the boundary curve of the image.

Similarly, we can derive the Euler-Lagrangian equation for ϕ_2.

$$\begin{aligned}\frac{\partial F_4}{\partial \phi_2} &= (c_{11}-u_0)^2\delta(\phi_2)H(\phi_1)-(c_{10}-u_0)^2H(\phi_1)\delta(\phi_2)\\&\quad+(c_{01}-u_0)^2\delta(\phi_2)(1-H(\phi_1))-(c_{00}-u_0)^2(1-H(\phi_1))\delta(\phi_2)\\&\quad+\nu\delta'(\phi_2)|\nabla\phi_1|\end{aligned} \tag{54}$$

and

$$\frac{\partial}{\partial x}(\frac{\partial F_4}{\partial \phi_{2x}}) = \nu[\delta'(\phi_2)\frac{\phi_{2x}^2}{\sqrt{\phi_{2x}^2+\phi_{2y}^2}} + \delta(\phi_2)\frac{\partial}{\partial x}\frac{\phi_{2x}}{\sqrt{\phi_{2x}^2+\phi_{2y}^2}}] \tag{55}$$

and

$$\frac{\partial}{\partial y}(\frac{\partial F_4}{\partial \phi_{2y}}) = \nu[\delta'(\phi_2)\frac{\phi_{2y}^2}{\sqrt{\phi_{2x}^2+\phi_{2y}^2}} + \delta(\phi_2)\frac{\partial}{\partial y}\frac{\phi_{2y}}{\sqrt{\phi_{2x}^2+\phi_{2y}^2}}] \tag{56}$$

Therefore, we have the following Euler-Lagrange equation for ϕ_2:

$$\begin{aligned}&\delta(\phi_2)\left[[(c_{11}-u_0)^2-(c_{10}-u_0)^2]H(\phi_1)+\right.\\&\left.[(c_{01}-u_0)^2-(c_{00}-u_0)^2](1-H(\phi_1))-\nu\nabla\cdot(\frac{\nabla\phi_2}{|\nabla\phi_2|})\right]=0\end{aligned} \tag{57}$$

with the boundary condition

$$\frac{\delta(\phi_2)}{|\nabla\phi_2|}\nabla\phi_2\cdot\hat{n}=\frac{\delta(\phi_2)}{|\nabla\phi_2|}\frac{\partial\phi_2}{\partial n}=0 \tag{58}$$

Here $\hat{n}$ is the normalized normal of the boundary curve of the image. Using the gradient projection method, we have the curve evolution equations for ϕ_1 and ϕ_2:

$$\begin{aligned}\frac{\partial\phi_1}{\partial t} &= \delta(\phi_1)\left[[-(c_{11}-u_0)^2-(c_{01}-u_0)^2]H(\phi_2)-\right.\\ &\quad \left.[(c_{10}-u_0)^2-(c_{00}-u_0)^2](1-H(\phi_2))+\nu\nabla\cdot(\frac{\nabla\phi_1}{|\nabla\phi_1|})\right]\\ \frac{\partial\phi_2}{\partial t} &= \delta(\phi_2)\left[[-(c_{11}-u_0)^2-(c_{10}-u_0)^2]H(\phi_1)-\right.\\ &\quad \left.[(c_{01}-u_0)^2-(c_{00}-u_0)^2](1-H(\phi_1))+\nu\nabla\cdot(\frac{\nabla\phi_2}{|\nabla\phi_2|})\right]\end{aligned} \tag{59}$$

Constants c_{11}, c_{10}, c_{01}, and c_{00} can be solved by:

$$\frac{\partial E}{\partial c_{11}}=0,\quad \frac{\partial E}{\partial c_{10}}=0,\quad \frac{\partial E}{\partial c_{01}}=0,\quad \frac{\partial E}{\partial c_{00}}=0. \tag{60}$$

Thus

$$c_{11}(\phi)=\frac{\int u_0H(\phi_1)H(\phi_2)dxdy}{\int H(\phi_1)H(\phi_2)dxdy} \tag{61}$$

$$c_{10}(\phi)=\frac{\int u_0H(\phi_1)(1-H(\phi_2))dxdy}{\int H(\phi_1)(1-H(\phi_2))dxdy} \tag{62}$$

$$c_{01}(\phi)=\frac{\int u_0(1-H(\phi_1))H(\phi_2)dxdy}{\int(1-H(\phi_1))H(\phi_2)dxdy} \tag{63}$$

$$c_{00}(\phi)=\frac{\int u_0(1-H(\phi_1))(1-H(\phi_2))dxdy}{\int(1-H(\phi_1))(1-H(\phi_2))dxdy} \tag{64}$$

If the image consists of more regions, we can use n level set functions to represent 2^n regions. So it is supposed that any number of regions can be segmented if enough level set functions are used. However, this is not true. First of all, the number of regions in an image is unknown before segmentation. We may use as many level set functions as possible to segment the image to avoid missing any regions. In this case, the evolutions of many curves are interlaced, and the computation

cost will be very large. The most important problem is that the MS energy functional is not convex. If many curves evolve simultaneously, the problem of initial condition will be more difficult to handle. To overcome these problems, we present a new hierarchical segmentation scheme in chapter five.

Chapter 4

Piecewise Linear Approximation and Modified Mumford-Shah Model

In this chapter, we present the piecewise linear approximation and the modified Mumford-Shah model to deal with the problem of creases and roof edges.

4.1 Piecewise Linear Approximation

The piecewise constant approximation can be used only when the intensities of objects in an image are uniform and can be approximated by constants. When the variance of intensity inside an object is large, the piecewise constant approximation will introduce larger errors. To adapt to the distribution of intensity inside object regions, we can use a linear function $u(x, y) = a + bx + cy$, instead of a constant, to approximate the intensity of an object. Here a, b, and c are constants.

For the case of two phases, we will have two linear functions, one approximating the inside, the

other approximating the outside of the level set curve:

$$u_1(x,y) = a_1 + b_1 x + c_1 y \tag{65}$$

$$u_2(x,y) = a_2 + b_2 x + c_2 y$$

Similar to equation (35), the MS energy functional can be written as:

$$\begin{aligned} E(a_i, b_i, c_i, \phi) &= \int (a_1 + b_1 x + c_1 y - u_0)^2 H(\phi) dxdy \\ &+ \int (a_2 + b_2 x + c_2 y - u_0)^2 (1 - H(\phi)) dxdy \\ &+ \mu(b_1^2 + c_1^2) \int H(\phi) dxdy + + \mu(b_2^2 + c_2^2) \int (1 - H(\phi)) dxdy + \\ &\nu \int |\nabla H(\phi)| dxdy. \end{aligned} \tag{66}$$

We define

$$\begin{aligned} F(\phi) &= (a_1 + b_1 x + c_1 y - u_0)^2 H(\phi) + (a_2 + b_2 x + c_2 y - u_0)^2 (1 - H(\phi)) \\ &+ \mu(b_1^2 + c_1^2) H(\phi) + \mu(b_2^2 + c_2^2)(1 - H(\phi)) + \nu\delta(\phi)|\nabla\phi|. \end{aligned} \tag{67}$$

Following the derivation of the Euler-Lagrange equation, we have

$$\begin{aligned} \frac{\partial F}{\partial \phi} &= (a_1 + b_1 x + c_1 y - u_0)^2 \delta(\phi) - (a_2 + b_2 x + c_2 y - u_0^2)\delta(\phi) + \\ &\mu(b_1^2 + c_1^2)\delta(\phi) - \mu(b_2^2 + c_2^2)\delta(\phi) + \nu\delta'(\phi)|\nabla\phi|] \end{aligned} \tag{68}$$

and

$$\frac{\partial}{\partial x}(\frac{\partial F}{\partial \phi_x}) = \nu[\delta'(\phi)\frac{\phi_x^2}{\sqrt{\phi_x^2 + \phi_y^2}} + \delta(\phi)\frac{\partial}{\partial x}\frac{\phi_x}{\sqrt{\phi_x^2 + \phi_y^2}}] \tag{69}$$

and

$$\frac{\partial}{\partial y}(\frac{\partial F}{\partial \phi_y}) = \nu[\delta'(\phi)\frac{\phi_y^2}{\sqrt{\phi_x^2 + \phi_y^2}} + \delta(\phi)\frac{\partial}{\partial y}\frac{\phi_y}{\sqrt{\phi_x^2 + \phi_y^2}}] \tag{70}$$

Thus, we have the following Euler-Lagrange equation:

$$\begin{aligned} &\delta(\phi)[-\nu\nabla \cdot \frac{\nabla\phi}{|\nabla\phi|} + (a_1 + b_1 x + c_1 y - u_0)^2 + \mu(b_1^2 + c_1^2) \\ &-(a_2 + b_2 x + c_2 y - u_0)^2 - \mu(b_2^2 + c_2^2)] = 0 \end{aligned} \tag{71}$$

with the following boundary condition

$$\frac{\delta(\phi)}{|\nabla\phi|}\nabla\phi\cdot\hat{n}=\frac{\delta(\phi)}{|\nabla\phi|}\frac{\partial\phi}{\partial n}=0. \tag{72}$$

Here $\hat{n}$ is the normalized normal of the boundary curve of the image.

Using the gradient projection method, we can change equaiton (71) to the following time dependent equation for $\phi(x,y,t)$

$$\begin{aligned}\frac{\partial\phi}{\partial t} &= \delta(\phi)[\nu\nabla\cdot\frac{\nabla\phi}{|\nabla\phi|}-(a_1+b_1x+c_1y-u_0)^2-\mu(b_1^2+c_1^2)\\ &\quad +(a_2+b_2x+c_2y-u_0)^2+\mu(b_2^2+c_2^2)]\end{aligned} \tag{73}$$

This is the evolution equation for segmentation curve.

We can calculate a_1, b_1, and c_1 via the following equations:

$$\frac{\partial E}{\partial a_1}=0,\frac{\partial E}{\partial b_1}=0,\frac{\partial E}{\partial c_1}=0. \tag{74}$$

or

$$\begin{aligned}&a_1\int H(\phi)dxdy+b_1\int H(\phi)xdxdy\\ &+c_1\int yH(\phi)dxdy=\int u_0H(\phi)dxdy\\ &a_1\int xH(\phi)dxdy+b_1\int[x^2+\mu]H(\phi)dxdy\\ &+c_1\int xyH(\phi)dxdy=\int xu_0H(\phi)dxdy\\ &a_1\int yH(\phi)dxdy+b_1\int xyH(\phi)dxdy+c_1\int[y^2+\mu]H(\phi)dxdy\\ &=\int yu_0H(\phi)dxdy\end{aligned} \tag{75}$$

Similar to the above, we can obtain the equations for a_2, b_2, and c_2, that is:

$$\frac{\partial E}{\partial a_2}=0,\frac{\partial E}{\partial b_2}=0,\frac{\partial E}{\partial c_2}=0. \tag{76}$$

Or

$$\begin{aligned}&a_2\int(1-H(\phi))dxdy+b_2\int(1-H(\phi))xdxdy\\ &+c_2\int y(1-H(\phi))dxdy=\int u_0(1-H(\phi))dxdy\end{aligned}$$

$$
\begin{aligned}
&a_2 \int x(1-H(\phi))dxdy + b_2 \int [x^2+\mu](1-H(\phi))dxdy \\
&+c_2 \int xy(1-H(\phi))dxdy = \int xu_0(1-H(\phi))dxdy \\
&a_2 \int y(1-H(\phi))dxdy + b_2 \int xy(1-H(\phi))dxdy + \\
&c_2 \int [y^2+\mu](1-H(\phi))dxdy = \int yu_0(1-H(\phi))dxdy
\end{aligned} \tag{77}
$$

Through solving the equations (73), (76), and (78), we can obtain the evolution of the level set curves and the final segmentation. In this process, only one PDE equation (73) needs to be solved. In every step of the iteration for solving the equation (73), we use equations (76) and (78) to update the constants a_1, b_1, c_1, a_2, b_2, and c_2.

The comparison between the segmentation results of the piecewise linear approximation and the piecewise constant approximation is shown in Figure 6. In Figure 6, we use two segmentation approaches: piecewise constant approximation and piecewise linear approximation, to segment an image of a head bone. The image is segmented into two regions and these two regions are represented by two constants or two planar functions in the reconstruction images (b) and (e) respectively. It is obvious that the piecewise linear approximation can detect more parts of the head bone. This is because the environmental lighting makes the image intensity of the head bone to vary, the top is lighter and the bottom is darker. In this case, a planar function can approximate the image intensity while the constant approximation leads to larger errors. This also is indicated by the MS energy in (c) and (f). The minimized MS energy of the linear approximation is much smaller than that of the constant approximation. Furthermore, because the linear approximation represents better the image intensity, the convergence speed of iteration for the linear approximation is much faster than that for the constant approximation.

The experiment in Figures 6 only segments the image into two regions, that is, two phases. To segment the image with more complicated structures, we need use two or more level set functions. For the four phase case, we use two level set functions to segment an image into four regions. The

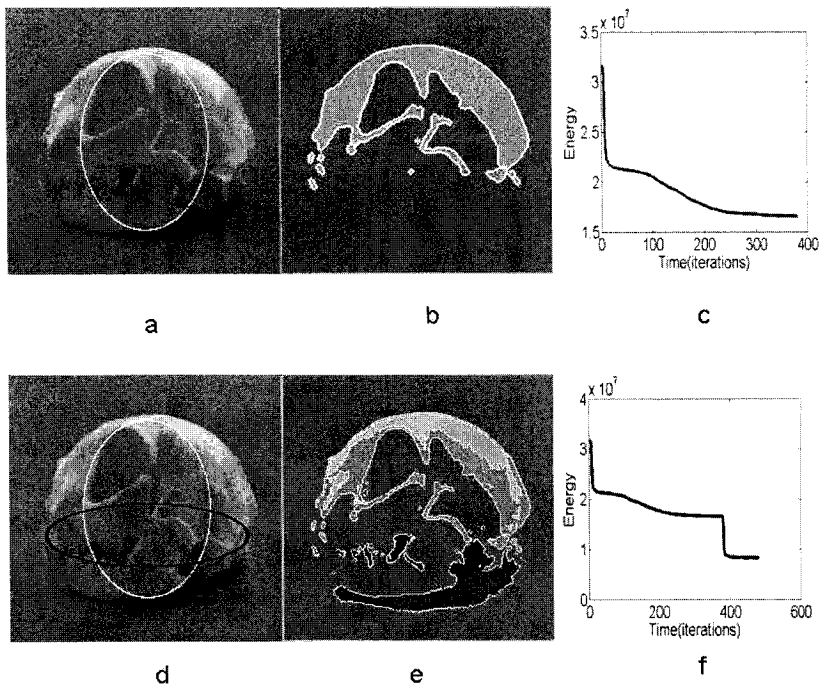

Figure 6: *Comparison between the segmentation results of the piecewise linear approximation and the piecewise constant approximation [29]. (a) Original image with the initial curve for the piecewise constant approximation; (b) The reconstruction image with the segmentation result of the piecewise constant approximation; (c) The MS energy versus the iteration time for the piecewise constant approximation; (d) Original image with the initial curve for the piecewise linear approximation; (e) The reconstruction image with the segmentation result of the piecewise linear approximation; (f) The MS energy versus the iteration time for the piecewise linear approximation.*

four regions can be approximated by four planar functions:

$$u_{11}(x,y) = a_{11} + b_{11}x + c_{11}y \tag{78}$$

$$u_{10}(x,y) = a_{10} + b_{10}x + c_{10}y$$

$$u_{01}(x,y) = a_{01} + b_{01}x + c_{01}y$$

$$u_{00}(x,y) = a_{00} + b_{00}x + c_{00}y$$

The MS energy functional becomes:

$$E_4^{linear}(a_{ij}, b_{ij}, c_{ij}, \phi_1, \phi_2) =$$

$$
\begin{aligned}
&\int (u_0 - a_{11} - b_{11}x - c_{11}y)^2 H(\phi_1)H(\phi_2)dxdy \\
&+ \int (u_0 - a_{10} - b_{10}x - c_{10}y)^2 H(\phi_1)(1 - H(\phi_2))dxdy \\
&+ \int (u_0 - a_{01} - b_{01}x - -c_{01}y)^2 (1 - H(\phi_1))H(\phi_2)dxdy \\
&+ \int (u_0 - a_{00} - b_{00}x - c_{00}y)^2 (1 - H(\phi_1))(1 - H(\phi_2))dxdy \\
&+\mu(b_{11}^2 + c_{11}^2) \int H(\phi_1)H(\phi_2)dxdy \\
&+\mu(b_{10}^2 + c_{10}^2) \int H(\phi_1)(1 - (H(\phi_2))dxdy \\
&+\mu(b_{01}^2 + c_{01}^2) \int (1 - H(\phi_1))H(\phi_2)dxdy \\
&+\mu(b_{00}^2 + c_{00}^2) \int (1 - H(\phi_1))(1 - (H(\phi_2))dxdy \\
&+\nu \int |\nabla H(\phi_1)|dxdy + \nu \int |\nabla H(\phi_2)|dxdy. \qquad (79)
\end{aligned}
$$

To minimize this MS energy functional, we need to solve the PDEs for the two curves, and the solutions of these PDEs are coupled. Therefore the computation cost will be large. To avoid this problem, we use the segmentation approach proposed in [2] to minimize the MS energy functional. In this approach, we first use one initial curve on the image and solve the one level set equation for the curve using equation (80):

$$
\begin{aligned}
\frac{\partial \phi_1}{\partial t} &= \delta(\phi_1)[-(a_1 + b_1 x + c_1 y - u_0)^2 - \mu(b_1^2 + c_1^2) \\
&\quad +(a_2 + b_2 x + c_2 y - u_0)^2 + \mu(b_2^2 + c_2^2) + \nu\nabla \cdot \frac{\nabla \phi_1}{|\nabla \phi_1|}] \qquad (80)
\end{aligned}
$$

Through the curve evolution, the curve will segment the image into two phases: $\phi_1 > 0$ for the inside region and $\phi_1 < 0$ for the outside region of the curves. Then we use the second level set curve ϕ_2 on the image. With the second curve, each of the two phases segmented by the first curve is now segmented by the second level set function. For the inside region 1 ($\phi_1 > 0$), we can solve the curve evolution of the second curve ϕ_2 by:

$$
\begin{aligned}
\frac{\partial \phi_2}{\partial t} &= \delta(\phi_2)[-(a_{11} + b_{11} x + c_{11} y - u_0)^2 - \mu(b_{11}^2 + c_{11}^2) \\
&\quad +(a_{10} + b_{10} x + c_{10} y - u_0)^2 + \mu(b_{10}^2 + c_{10}^2) + \nu\nabla \cdot \frac{\nabla \phi_2}{|\nabla \phi_2|}] \qquad (81)
\end{aligned}
$$

And for the outside region 2 ($\phi_1 < 0$)), the curve evolution equation of the second curve ϕ_2 is:

$$\begin{aligned}\frac{\partial \phi_2}{\partial t} &= \delta(\phi_2)[-(a_{01}+b_{01}x+c_{01}y-u_0)^2-\mu(b_{01}^2+c_{01}^2) \\ &\quad +(a_{00}+b_{00}x+c_{00}y-u_0)^2+\mu(b_{00}^2+c_{00}^2)+\nu\nabla\cdot\frac{\nabla\phi_2}{|\nabla\phi_2|}] \end{aligned} \tag{82}$$

We can obtain the segmentation through the solution of the three PDEs (80), (81), and (82). Because the solutions of the three PDEs are decoupled, the computation will be much faster than the direct solution of equation (79).

A segmentation example of the four phase case is shown in Figure 7. In Figure 7, the segmentation

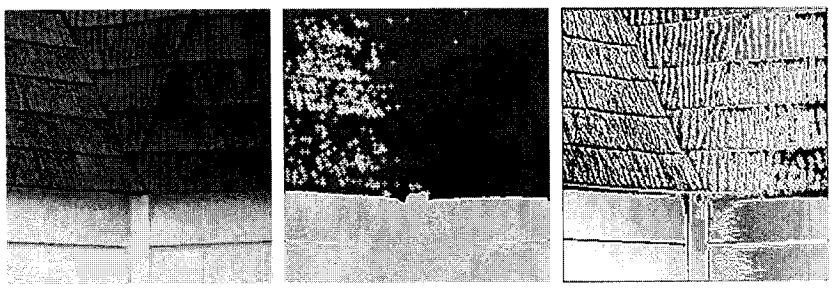

Figure 7: *Segmentation of the four phase case [29]. From left to right: The first is the original image; the second is the segmentation result by the piecewise constant approximation of the MS model; the third is the segmentation result by the linear approximation.*

results by both the piecewise constant approximation and the piecewise linear approximation are shown. It is obvious that the linear approximation approach can produce better segmentation. This is because the linear approximation can adapt to the intensity distribution of the objects.

4.2 ROF Mumford-Shah Model

In the MS model, the regularization term (second term) is small in object regions, but is large across the boundaries. Therefore the original MS model can be used to detect discontinuities in the image surface. While the MS model works well in many applications, there are two cases that are difficult for the MS approach. One is the detection of low contrast edges. This is because the L^2-norm of the gradient term in the MS energy functional is too large for edges. The minimization of the MS energy functional will remove low contrast edges. Different from the classical MS energy

model, Rudin, Osher and Fatemi (ROF) [13] changed L^2-norm to L^1-norm and modeled the energy functional as follows:

$$E(u, C) = \int_{\Omega \setminus C} |u - u_0|^2 dxdy + \mu \int_{\Omega \setminus C} |\nabla u| dxdy + \nu |C|, \tag{83}$$

In this model, L^1-norm of the gradient can preserve low contrast edges.

Zhang in [29] presented a piecewise constant approximation approach to solve this model. Because the gradient term disappears in the constant approximation, [29] added the gradient of the original image u_0 in the MS energy functional to detect low contrast edges. The MS energy functional used in [29] is:

$$\begin{aligned} E(u, C) = & \int_{inside\ C} (c_1 - u_0)^2 dxdy + \int_{outside\ C} (c_2 - u_0)^2 dxdy \\ & + \mu \int_{inside\ C} |\nabla u_0| dxdy + \nu |C| \end{aligned} \tag{84}$$

In this model, [29] only calculated the gradient inside C. The advantage of this approximation compared to the original ROF model is that the calculation is faster since we do not need to solve two coupled PDEs for u inside and outside, respectively.

The level set function equation becomes:

$$\frac{\partial \phi}{\partial t} = -\delta(\phi)[(c_1 - u_0)^2 - (c_2 - u_0)^2 + \mu |\nabla u_0| - \nu \nabla \cdot (\frac{\nabla \phi}{|\nabla \phi|})], \tag{85}$$

Comparison between the classical MS model and the improved ROF model is shown in Figure 8. In Figure 8, it is obvious that the modified ROF model can detect more edges in the image compared to the classical MS model.

4.3 Modified Mumford-Shah Model with Second Order Derivative Term

Another difficulty with the classical MS model is the detection of roof edges. For roof edges, the gradient of u is not small in the regions on both sides of the roof edge, but the second order derivatives

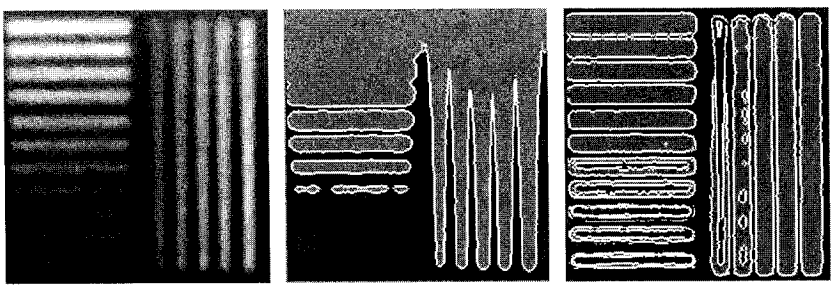

Figure 8: *Comparison of segmentation results using the classical MS model and the modified ROF model using the piecewise constant approximation [29]. From left to right: the first is the original image; the second is the segmentation result of the MS model; the last is the segmentation result of the modified ROF mode.*

of u is small, and the gradient of u is discontinuous across the boundary. That is there is a step edge in the first order derivative functional space. To minimize the classical MS energy functional, the gradient of u inside the segmented regions is forced to be small, but this will make it difficult to detect roof edges. To overcome this difficulty, we modify the MS model to following form:

$$E(u, C) = \int_{\Omega \setminus C} (u - u_0)^2 dxdy + \lambda \int_{\Omega \setminus C} |\Delta u|^2 dxdy + \int \nu |C| \tag{86}$$

In the following, we will denote equation (86) as the modified Mumford-Shah (MMS) model. In MMS we ignore the gradient term because this term forces the gradient of u to be small inside each region, but this is not true for roof edges. If we include this term, we will miss the roof edges. On the other hand, we add the term of the second order derivative of u. Because the second order derivative of u is small inside regions and large across both step edges and roof edges, minimizing the second order derivative term in MMS model can detect both step edges and roof edges.

The authors of [38] introduced an energy with second order derivative term as following:

$$\begin{aligned} E(u, K_0, K_1) = & \int_{\Omega \setminus (K_0 \cup K_1)} (|\Delta u|^2 + \phi(x, u)) dx \\ & + \alpha \mathcal{H}^{n-1}(K_0 \cap \Omega) + \beta \mathcal{H}^{n-1}((\mathrm{K}_1 \setminus \mathrm{K}_0) \cap \Omega) \end{aligned} \tag{87}$$

where α, β are positive parameters; $\mathcal{H}^{(n-1)}$ is the Hausdorff $(n-1)$-dimensional measure. K_0 represents the set of jump points for u (step edges), and $K_1 \setminus K_0$ is the set of crease points (roof edges).

Actually, the MMS model is a special case of equation (87). When $\phi(x,u) = \mu|u-u_0|^2$ and $\alpha = \beta$, equation (87) is equivalent to the MMS model.

Finding the solution of MMS model for an arbitrary image is more difficult than for the MS model. The authors in [38] used elliptic functional approximation to solve equation (87). In this thesis, we use level set function and piecewise linear approximation to solve equation (86). Compared with the approach in [38], our approach is more simple and faster.

For roof edges, the gradient of u is not small inside the segmented regions, and the image intensity varies inside these regions. So the piecewise constant approximation is not suitable for this case. If we use piecewise constant approximation approach, one region could be segmented into several regions as seen in Figure 22. To conserve the information of the gradients, we use the piecewise linear approximation. With the piecewise linear approximation, we define

$$u_1(x,y) = a_1 + b_1 x + c_1 y \tag{88}$$

$$u_2(x,y) = a_2 + b_2 x + c_2 y$$

The MMS model can be written as:

$$\begin{aligned} E(a_i,b_i,c_i,\phi) &= \int (a_1 + b_1 x + c_1 y - u_0)^2 H(\phi) dxdy \\ &\quad + \int (a_2 + b_2 x + c_2 y - u_0)^2 (1 - H(\phi)) dxdy \\ &\quad + \nu \int |\nabla H(\phi)| dxdy. \end{aligned} \tag{89}$$

In equation (89), the second derivative term of u disappears because of the linear approximation.

We define

$$F(\phi) = (a_1 + b_1 x + c_1 y - u_0)^2 H(\phi) + (a_2 + b_2 x + c_2 y - u_0)^2 (1 - H(\phi)) + \nu\delta(\phi)|\nabla\phi|. \tag{90}$$

Following the derivation of the Euler-Lagrange equation, we have

$$\frac{\partial F}{\partial \phi} = (a_1 + b_1 x + c_1 y - u_0)^2 \delta(\phi) - (a_2 + b_2 x + c_2 y - u_0^2)\delta(\phi) + \nu\delta'(\phi)|\nabla\phi|] \tag{91}$$

and

$$\frac{\partial}{\partial x}\left(\frac{\partial F}{\partial \phi_x}\right) = \nu[\delta'(\phi)\frac{\phi_x^2}{\sqrt{\phi_x^2 + \phi_y^2}} + \delta(\phi)\frac{\partial}{\partial x}\frac{\phi_x}{\sqrt{\phi_x^2 + \phi_y^2}}] \tag{92}$$

and

$$\frac{\partial}{\partial y}(\frac{\partial F}{\partial \phi_y}) = \nu[\delta'(\phi)\frac{\phi_y^2}{\sqrt{\phi_x^2+\phi_y^2}} + \delta(\phi)\frac{\partial}{\partial y}\frac{\phi_y}{\sqrt{\phi_x^2+\phi_y^2}}] \tag{93}$$

Thus, we have the following Euler-Lagrange equation:

$$\delta(\phi)[-\nu\nabla\cdot\frac{\nabla\phi}{|\nabla\phi|} + (a_1+b_1x+c_1y-u_0)^2 - (a_2+b_2x+c_2y-u_0)^2] = 0 \tag{94}$$

with the following boundary condition.

$$\frac{\delta(\phi)}{|\nabla\phi|}\nabla\phi\cdot\hat{n} = \frac{\delta(\phi)}{|\nabla\phi|}\frac{\partial\phi}{\partial n} = 0. \tag{95}$$

Here $\hat{n}$ is the normalized normal of the boundary curve of the image.

Using the gradient projection method, we can change equation (94) to the following time dependent equation for $\phi(t)$

$$\frac{\partial\phi}{\partial t} = \delta(\phi)[\nu\nabla\cdot\frac{\nabla\phi}{|\nabla\phi|} - (a_1+b_1x+c_1y-u_0)^2 + (a_2+b_2x+c_2y-u_0)^2] \tag{96}$$

This is the evolution equation for segmentation curve.

We can calculate a_1, b_1, and c_1 via the following equations:

$$\frac{\partial E}{\partial a_1} = 0, \frac{\partial E}{\partial b_1} = 0, \frac{\partial E}{\partial c_1} = 0. \tag{97}$$

or

$$\begin{aligned}
&a_1\int H(\phi)dxdy + b_1\int H(\phi)xdxdy \\
&+c_1\int yH(\phi)dxdy = \int u_0H(\phi)dxdy \\
&a_1\int xH(\phi)dxdy + b_1\int x^2H(\phi)dxdy \\
&+c_1\int xyH(\phi)dxdy = \int xu_0H(\phi)dxdy \\
&a_1\int yH(\phi)dxdy + b_1\int xyH(\phi)dxdy + c_1\int y^2H(\phi)dxdy \\
&= \int yu_0H(\phi)dxdy
\end{aligned} \tag{98}$$

Similar to the above, we can obtain the equations for a_2, b_2, and c_2, that is:

$$\frac{\partial E}{\partial a_2} = 0, \frac{\partial E}{\partial b_2} = 0, \frac{\partial E}{\partial c_2} = 0. \tag{99}$$

or

$$
\begin{aligned}
&a_2 \int (1 - H(\phi))dxdy + b_2 \int (1 - H(\phi))xdxdy \\
&+c_2 \int y(1 - H(\phi))dxdy = \int u_0(1 - H(\phi))dxdy \\
&a_2 \int x(1 - H(\phi))dxdy + b_2 \int x^2(1 - H(\phi))dxdy \\
&+c_2 \int xy(1 - H(\phi))dxdy = \int xu_0(1 - H(\phi))dxdy \qquad (100) \\
&a_2 \int y(1 - H(\phi))dxdy + b_2 \int xy(1 - H(\phi))dxdy + \\
&c_2 \int y^2(1 - H(\phi))dxdy = \int yu_0(1 - H(\phi))dxdy
\end{aligned}
$$

The segmentation of an artificial roof edge is shown in Figure 9. In Figure 9, the piecewise

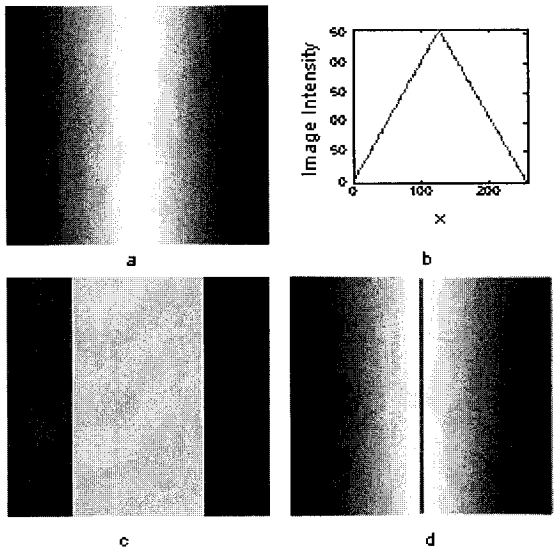

Figure 9: *Segmentation of an artificial roof edge. (a) Original image; (b) Image intensity distribution along horizontal direction; (c) Segmentation result by the piecewise constant approximation of the MS model; (d) Segmentation result by linear approximation of the MMS model.*

constant approximation of the MS model segments the image into three regions and cannot detect the roof edge. On the contrary, the linear approximation of the MMS model can detect the roof edge. This is because the gradient inside each region is a constant, that is, the second order derivative is small inside each region, and the second order derivative is large across the roof edge.

Chapter 5

Hierarchical Segmentation

In this chapter, we present a new hierarchical segmentation scheme to detect both main structures and details of an image.

5.1 Introduction

With the level set method, the MS model works well in many applications. However, generally only one or two level set functions are used to segment an image into two or four phases. Therefore, most experiments are done on simple images. For images with complicated structures, the regions in the images cannot be represented by one or two level set functions. We need n level set functions to represent 2^n regions. There are three difficulties for this approach. First, we cannot define the number of regions before hand. We may use many level set functions to segment an image to avoid missing any region. However this approach requires large computational cost. The most important problem for the MS model using the level set method is the initial condition. Because the MS energy functional is not convex, the minimization result often is trapped by a local minimum. Consequently the segmentation result depends on the initial conditions. This problem is more serious for the cases with many level set functions. As a result, generally the MS model can only detect the main structure of an image rather than detailed segmentation.

To segment the images with complicated structures, [1] and [2] presented hierarchical segmentation approaches. The basic idea of the hierarchical segmentation approach proposed in [1] is as follows: First, put an arbitrary initial closed curve in the image. Through the evolution, the curve will segment the image into two or more regions. Because in the evolution, the closed curve could split into two or more closed curves, the segmentation result could consist of more than two regions. In the second stage, put another arbitrary initial closed curve in each region obtained from the previous segmentation. Then through curves evolution, the curves inside each region will segment the region into more regions. We can put more curves into regions obtained from the last segmentation stage and segment the image into more regions. In this way, we can segment the image into any number of regions. The difference between [1] and [2] is the following: after one segmentation stage, [1] puts a second curve over all regions, instead of one curve in one region, and segments all the regions simultaneously. The disadvantages of these two approaches include:

1. In the approach in [2], we cannot decide if one region needs more additional segmentations, and there is no stopping criterion. On the other hand, the stopping criterion mentioned in [1] suggests that this hierarchical segmentation process will stop when the new segmentation will not change the MS energy functional. Because the segmentation results depend on the initial conditions, whether the MS energy of the new segmentation is smaller than the original MS energy depends on the initial conditions. Even when the MS energy of the new segmentation is not smaller than the original MS energy, it is still possible that the region needs additional segmentations. So this stopping criterion cannot guarantee the final segmentation result.

2. Although the hierarchical segmentation approaches in [1] and [2] can segment an image into many regions, these approaches cannot guarantee the segmentation is correct. Because the MS energy functional is not convex, it is possible that the segmentation curves do not reach the boundaries of objects, and one object may be segmented into several regions, i.e. the image is over segmented.

3. Tsai et al. in [1] indicated that their hierarchical segmentation approach cannot be used for

automatic image segmentation. In fact, the hierarchical approach in [1] is more suitable for denoising than for locating the segmentation curves. On the other hand, the segmentation approach in [2] can run automatically. However, because there is no stopping criterion, [2] only uses two segmentation stages to segment some relative simple images.

For images with complicated or detailed structures, although the MS model can produce segmentation results for the main structures, local segmentation approaches can produce better results for detailed structures. To combine the advantages of these two kinds of approaches, we present a new hierarchical segmentation scheme which makes use of both global and local information. In the process of the hierarchical segmentation, we use a local window (a small area of image intensity) over a segmentation region to detect whether the region needs additional segmentations or not. In this way, we can segment the image hierarchically until each object region is smooth. As a result, we can keep the segmentation of the main structures, and we also can detect detailed structures. The most important advantage of this approach is that the segmentation result does not depend on the initial conditions and the method is relatively fast.

5.2 Hierarchical Segmentation Scheme

Before the discussion of our new hierarchical segmentation scheme, we need to clarify the concept of an object. In an image, what should be considered as an object that needs to be segmented? In reality, the object should be meaningful. However, without any prior knowledge, it is difficult to define objects in an image. In this paper, we define an object as an area of image intensity with a certain level of contrast to its background in the image. The object should meet two conditions: the area of the object should be bigger than a threshold T_a, and the absolute difference between the average object image intensity and its background should be bigger than a threshold T_c. The goal of segmentation is to segment an image into different objects from their background.

We now present our new hierarchical segmentation scheme as follows:

1. Define an initial closed curve. The area inside the curve corresponds to the area threshold T_a.

2. Move the initial curve to different positions in one region (in the beginning, the region is the whole image), and calculate the average intensities inside the curve and the whole region. If at any position, the absolute difference between the two average intensities is smaller than the contrast threshold T_c, the region needs no more segmentation. Otherwise, position the initial curve at the location where the absolute difference is the largest.

3. In the region (in the beginning, the region is the whole image), use piecewise constant or linear approximation of the MS model to solve the curve evolution and obtain the segmentation result.

4. Number the different regions in the image.

5. In each region, repeat steps 2 and 3 to segment the region into smaller regions. In this step, all the calculations are inside one region.

6. Repeat 5 for each region obtained from different segmentation stages until all regions need no more segmentation.

7. Calculate the average intensity of each region. If the absolute difference between the average intensities of two neighbor regions is smaller than the contrast threshold used in step 2, T_c, the two regions are merged into one region.

8. Calculate the area of each region. If the area is too small, for example less than 10 pixels, the region is regarded as noise, and is merged into its neighboring region.

To detect all the details of an image, we can define the minimum object area as one pixel. If there exists noise, however, the noise can also be detected as an object. Therefore, in step 1 we need to define a minimum object area to avoid the effect of noise. For step 2, it is obvious that if the absolute differences between the probe areas and the background are smaller than the contrast threshold, there is no object in the region, and the region needs no more additional segmentations. If at some positions, the difference is bigger than the contrast threshold, we position the initial level

set curve at the location where the difference is the largest. At this location, the MS energy of the initial curve is the smallest compared to all other locations.

Repeat steps 2 and 3 on all regions until no more segmentation is needed in each region. At this point, each region is smooth enough. However, this is not the final result. Because the curve evolution of segmentation does not guarantee that the curve reaches the boundary of an object. It is possible that an object is segmented into more than one region. In this case, we can merge those neighboring regions whose average intensities are similar. After merging, the image intensity changes smoothly inside the objects and the boundaries are kept because the neighboring regions with large differences are not merged. The threshold used in this step is the same as the contrast threshold used in step 2.

In step 8, we remove those regions with very small area, which are assumed to be noise instead of object.

The flow chart of the hierarchical segmentation scheme is shown in figure 10

In this segmentation scheme, we need to define two important parameters, the area threshold and the contrast threshold of the objects. As mentioned before, we must define the objects for segmentation. Without the definition of the objects, we cannot define the real segmentation result. These two parameters can be obtained from the observation of an image. In the classical MS model, we need not define these two thresholds. Instead, we need to define parameter ν and μ. In the piecewise constant approximation, μ disappears, and ν becomes the only parameter. The authors in [2] suggest that ν is proportional to the variance σ^2 of an image. They also suggest a proportional ratio range. In this paper, we prefer to calculate ν from the contrast threshold in the object definition. In the following, we present the relationship between ν and the contrast threshold T_c.

As shown in figure 11, if the region can be segmented, we use R_2 to represent the region of an object and R_1 to represent the background region. The MS energy functional is:

$$E_a = \int_{R_1} (c_1 - u_0)^2 dxdy + \int_{R_2} (c_2 - u_0)^2 dxdy + \nu L \tag{101}$$

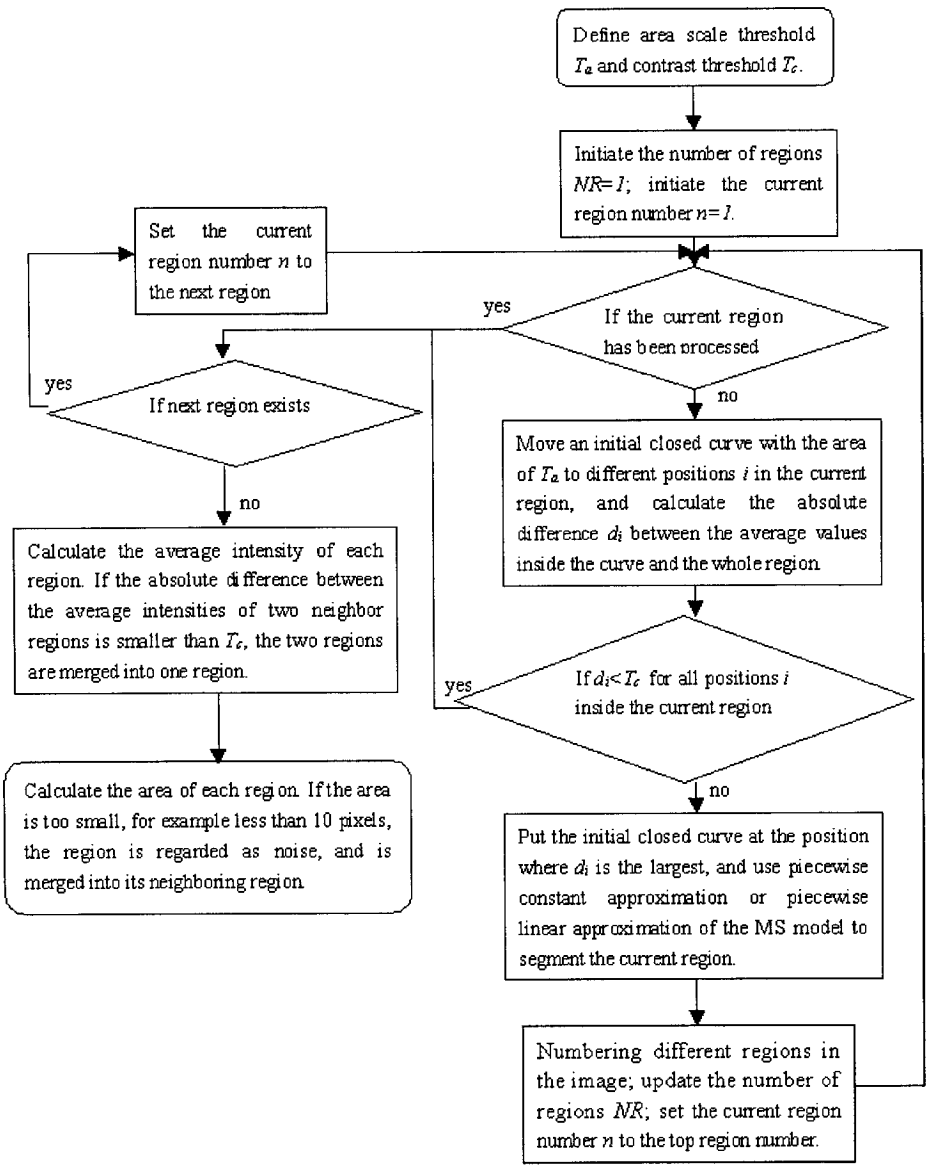

Figure 10: *The flow chart of the hierarchical segmentation scheme.*

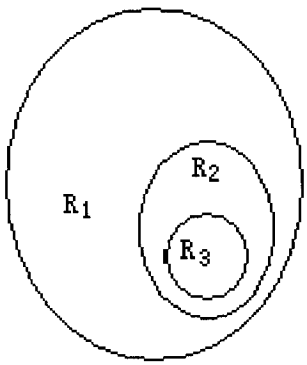

Figure 11: *Criterion for the smoothness of segmentation regions.*

where c_1 is the average intensity of the background region R_1; c_2 is the average intensity of the object region R_2; L is the length of the segmentation boundary. We assume the image intensity inside R_2 is uniform and can be approximated by a constant c_2, and we ignore the second term in equation (101). On the contrary, if there are some other objects inside R_1, the image intensity over R_1 is not uniform, and the first term should be kept. So the MS energy functional can be written as:

$$E_a = \int_{R_1} (c_1 - u_0)^2 dxdy + \nu L \tag{102}$$

Correspondingly, the MS energy functional for the whole region without any segmentation is:

$$E_b = \int_{R_1+R_2} (c_0 - u_0)^2 dxdy + \nu L \tag{103}$$

where c_0 is the average intensity of whole region $R_1 \cup R_2$. The relationship between c_1 and c_0 can be written as equation (104).

$$c_1 = \frac{c_0(A_1 + A_2) - c_2 A_2}{A_1} \tag{104}$$

where A_1 and A_2 are the areas of the background region R_1 and the object region R_2 respectively. If the region can be segmented, the MS energy functional after the segmentation should be smaller

than that of the original region, that is,

$$E_a < E_b \tag{105}$$

Substituting equations (102), (103) and (104) into equation (105), we can obtain:

$$\nu < \frac{A_2 A_0}{(A_0 - A_2)L}(c_2 - c_0)^2 \tag{106}$$

If the initial curve R_3 is inside R_2 as shown in figure 11, the average intensity inside R_3 can be approximated by R_2 because the image intensity inside R_2 is uniform. Therefore, the minimum value of $c_2 - c_0$ is the contrast threshold used in the object definition, T_c.

When the shape of region R_2 is a line, the boundary length L of the region is $2A_2$, which is the maximum value of L. So $L < 2A_2$.

If

$$\nu < \frac{A_0}{2(A_0 - A_2)}T_c^2 \tag{107}$$

then equation (106) is valid.

If we assume $A_2 << A_0$, then equation (107) becomes:

$$\nu < \frac{T_c^2}{2} \tag{108}$$

We can use equation (108) to estimate ν from the contrast threshold. In our experiments, $\nu < T_c^2/2$.

While most papers define ν directly, we believe that it is more reasonable to estimate ν from the minimum object contrast because the contrast can be observed from the image itself. To define T_c, we first find the object with the lowest contrast to the background in the image through observation. Then we calculate the average intensities of the object and its neighbor background respectively. T_c is estimated as the absolute difference between these two values. For the images with large object contrast and little noise, as long as T_c is in a range, we can obtain good segmentation results. Therefore, it is easy to define T_c in this case. However, it is difficult to define T_c for the images with low contrast and large noise. T_c must be defined accurately; otherwise, some objects with low contrast could be missed, or some noise could be detected as objects. In this case, we can only

roughly estimate T_c through observation. The accurate value sometimes has to be defined through some segmentation experimentations.

Figure 12 shows the dependency of the segmentation results on the initial condition if we use the classical piecewise constant approximation.

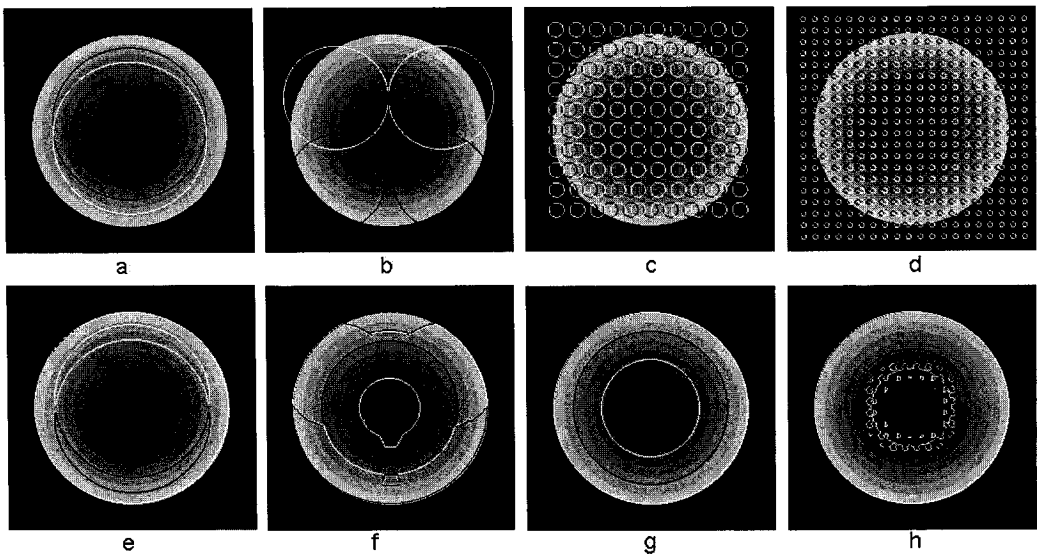

Figure 12: *Segmentation of concentric circles using two level set functions and the classical piecewise approximation. Top row: initial curves; bottom row: segmentation results.*

In Figure 12, we use Chan-Vese's piecewise constant approximation approach in [4] with 2 level set functions and different initial curves to segment the image. The segmentation results are different. Even in the best case (g), many circles are not segmented. On the contrary, we obtain the correct segmentation of the image using the new hierarchical segmentation scheme in Figure 13. Figure 13 also shows the different stages of the segmentation. Figure 13 (a) shows the initial curve and the original image; Figures 13 (b - g) show intermediate stages of our hierarchical method. The stages between (c) and (d) are not shown in the figure. Figure 13 (h) is the final result. The initial curves of different stages can be located automatically, and after evolution, they segment the image or large regions into smaller regions. Finally, the segmentation stops at the best segmentation according to the criterion presented in this paper.

If we use piecewise linear approximation to segment every regions in step (3), we can also detect

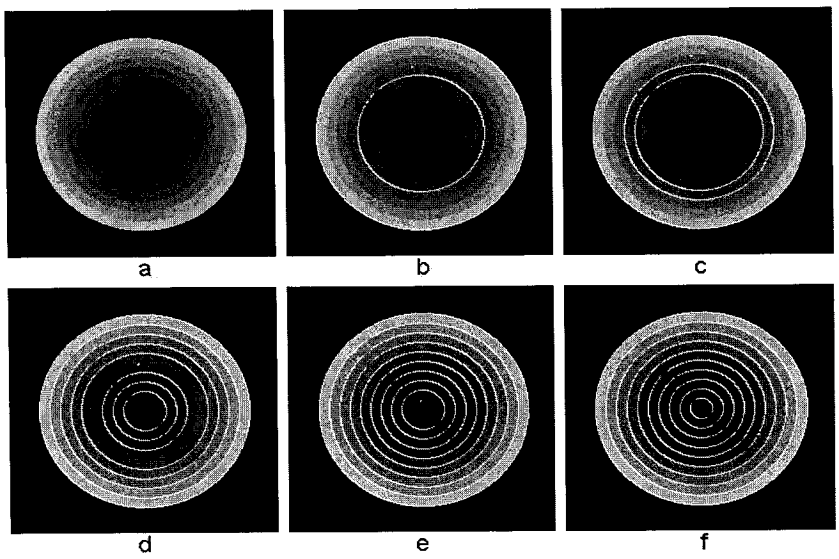

Figure 13: *Hierarchical segmentation of circles. Minimum scale:* 3×3, *minimum object contrast:* 5

roof edges. If we use piecewise linear approximation and the MMS method with different initial conditions to segment an artificial roof edge similar as Figure 15, the segmentation result depends on the initial conditions and no correct segmentation can be obtained. On the contrary, in Figure 15, we use our new hierarchical segmentation scheme to segment the same image, we can obtain the correct segmentation. Figure 15 (b) is the segmentation result before the merging of neighboring regions with similar image intensity. After merging, we obtain the correct segmentation.

For roof edges, we use piecewise linear approximation instead of constant approximation. In this case, we need to compare three values of the two neighbor regions to decide if these regions should be merged. On the segmentation boundary between the two regions, if the absolute difference between the reconstructed values calculated by the two planar functions to approximate the two regions is smaller than the contrast threshold T_c, the image intensity is continuous across the boundary. This is the first condition for merging. To merge two neighboring regions, the distribution slopes of the two regions also should be similar. That is, if the two planar functions of the two regions are represented by $u_1(x, y) = a_1 + b_1 x + c_1 y$ and $u_2(x, y) = a_2 + b_2 x + c_2 y$ respectively, $|a_1 - a_2| < T_s$ and $|b_1 - b_2| < T_s$, where T_s is a slope threshold defined for the roof edge. In addition to T_c, which

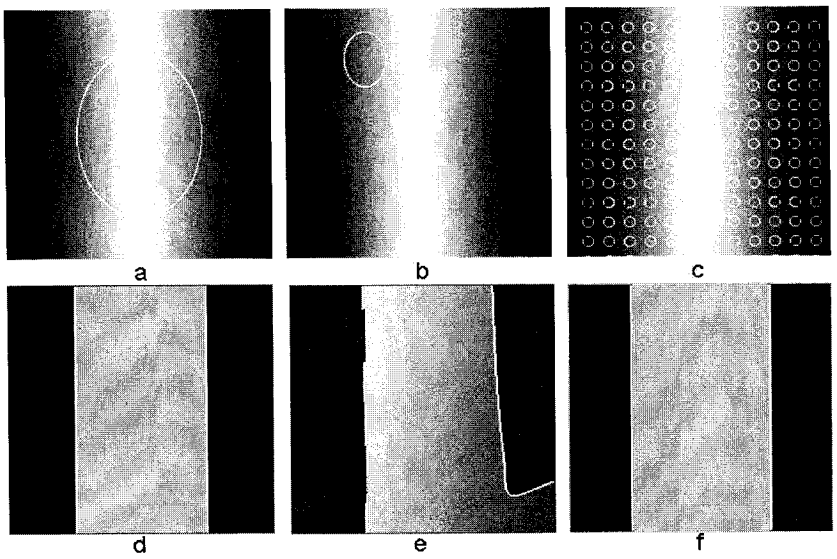

Figure 14: *Segmentation of roof edge using different initial curves and the piecewise linear approximation. Top row: initial curves; bottom row: segmentation results.*

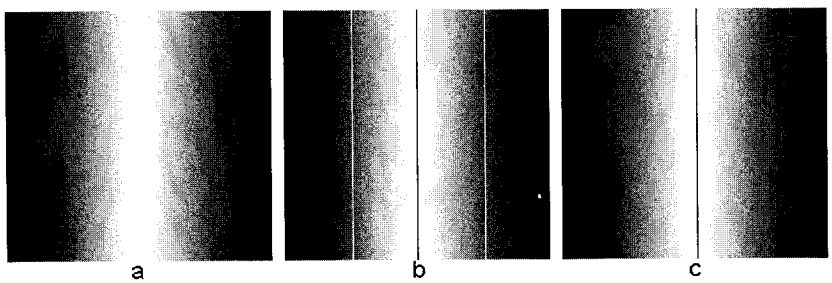

Figure 15: *Segmentation result of roof edge using our hierarchical segmentation scheme. (a) Original image; (b) Segmentation result before merging regions; (c) Final segmentation result.*

can be defined by the same way for step edges, we need to define another parameter T_s for roof edges. Through the observation of the image, we find the roof edge with the lowest slope difference, and we define T_s as this difference.

Chapter 6

Experimental Eesults for Hierarchical Segmentation Scheme

In this chapter, more segmentation results are shown to indicate that the new hierarchical segmentation scheme is valid in many cases.

Figure 16 shows segmentation results using the two level-set functions and Chan-Vese's method [4] on a medical image. It is obvious that the result depends on the initial curve. Figure 16 (f) is the best result. Even in this case many boundaries are missing and many pixels are segmented as regions although they are not.

Figure 17 (b) and (c) show the results using the segmentation approach proposed in [2]. With the approach in [2], we need to adjust the parameters by experimentation. Even in the optimal results shown in (b) and (c), there are many noise speckles and some edges are missed. On the contrary, the segmentation results of the new hierarchical scheme presented in this paper are much better. Figure 17 (c) is the result after 6 steps of the new hierarchical segmentation scheme. In this figure, almost all the boundaries of objects are detected, but some objects are segmented into several regions. Also there are some noise speckles inside some objects. At this point, the image is over segmented. After merging neighboring regions with similar averages, and removing the noise speckles as in step (7)

and (8) of the algorithm, the final result shown in Figure 17 (d) is much better.

Two more segmentation results are shown in Figure 18 and 19. In Figure 18, the tomogram of body is segmented into different regions according to the image intensity. In Figure 19, the segmentation result using our hierarchical segmentation scheme, Figure 19 (f), is much better than the results using the hierarchical segmentation approach proposed in [2] and shown in Figure 19 (c). Our result can detect correct boundaries, and even can detect the white materials in the brain with very complicated shape. In addition, there are no noise speckles in our result.

The MS model can also be used to denoise images. We first segment the image, and based on the segmentation result, smoothing is implemented inside each region but not across the boundaries. In this way, the noise is removed inside objects, but the boundaries of objects are kept untouched. This approach is proposed by [2]. Compared with the classical MS denoise approach, in which the segmentation and denoise are implemented at the same time, this approach decouples the segmentation and denoise processes hence decreases the computational cost. In our implementation, we first use the new hierarchical segmentation scheme to segment the image, then use Gaussian filter to smooth each region. The results are shown in Figures 20 and 21.

In Figures 20 and 21, Chan-Vese's approach in [4] and the hierarchical approach in [2] can only detect large structure of the image and miss many details. Consequently, many details are smoothed out in the denoise process. On the contrary, our new hierarchical scheme can detect details in image even in the case that noise is very strong, such as in Figure 21 with SNR=10. The white materials inside brain is very clear in Figure 21 (d).

Figure 22 shows the comparison between the segmentation results using constant and linear approximations. In both (b) and (c), we use our new hierarchical segmentation scheme to segment the image; (b) is for the constant approximation, and (c) is for the linear approximation. In (b), the region of the cheek is segmented into several regions. However in (c), the region is kept as one. This is because the linear approximation can adapt to the intensity variations.

Figure 23 shows the segmentation results using different minimum object area. With decreasing

scales, the detected regions become smaller and more details are detected. While the main parts of brain are segmented when scale=21, details of every parts are detected when scale=5. However, noise also are segmented as objects when the scale is too small. The reconstructed images are also shown in the figure. In the reconstructed images, the image intensity inside each region is represented by the average of the region. Obviously, more details are shown with the decreasing of the scale.

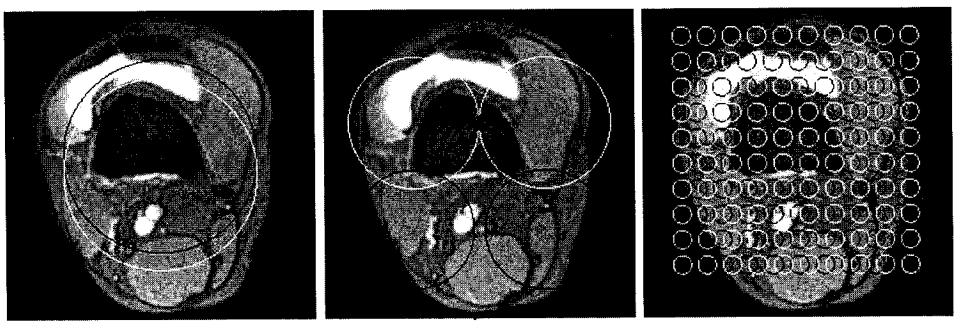

(a) Image with initial curve 1 (b) Image with initial curve 2 (c) Image with initial curve 3

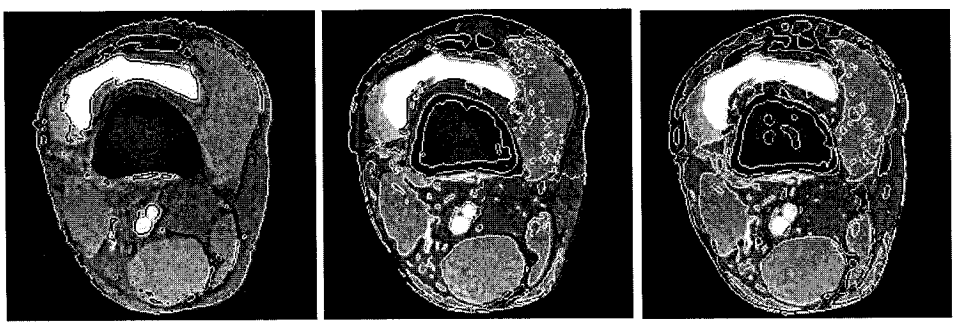

(d) Segmentation result of initial curve 1 (e) Segmentation result of initial curve 2 (f) Segmentation result of initial curve 3

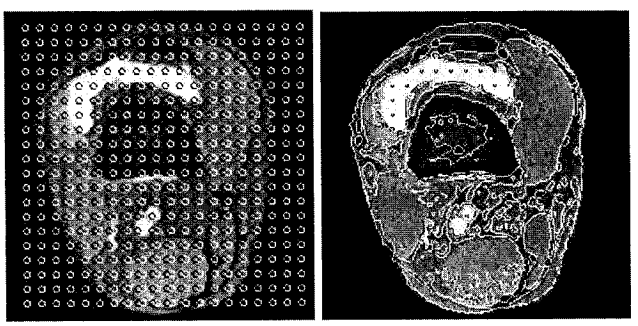

(g) Image with initial curve 4 (h) Segmentation result of initial curve 4

Figure 16: *The segmentation of knee using two level set functions and the Chan-Vese method.*

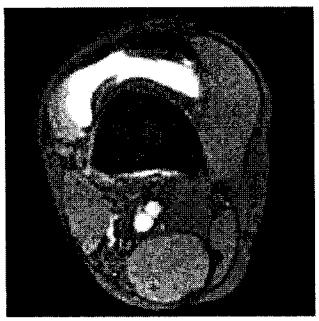

(a) Original image.

(b) Segmentation result using approach in [2] with parameter 1.

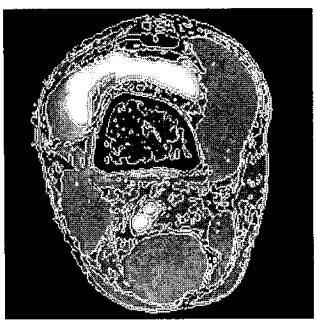

(c) Segmentation result using approach in [2] with parameter 2

(d) Segmentation result using hierarchical segmentation scheme before merging regions and deleting noise region.

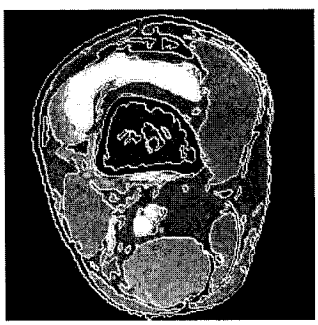

(e) Final segmentation result using hierarchical segmentation scheme.

Figure 17: *Segmentation result of knee. Minimum scale:* 21×21*; minimum object contrast:* 7

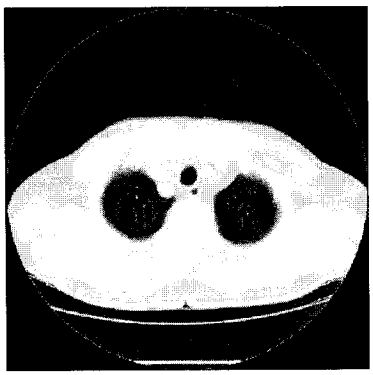

(a) Original image.

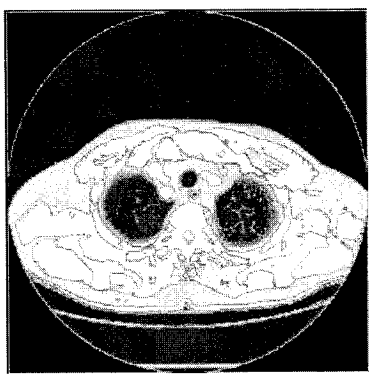

(b) Segmentation result before merging regions and removing noise speckles.

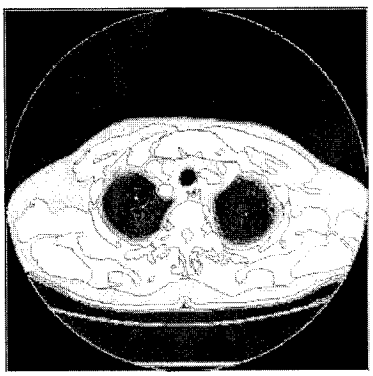

(c) Final segmentation result.

Figure 18: *Segmentation result of lung. Minimum scale:* 15×15*; minimum object contrast:* 7

(a) Original image.

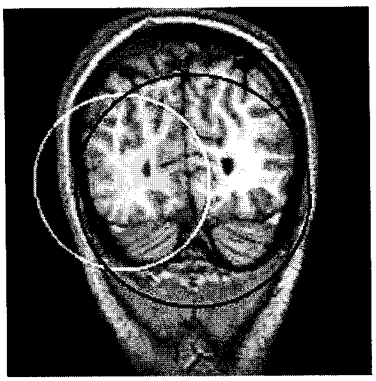

(b) Two initial curves for the segmentation approach in [2].

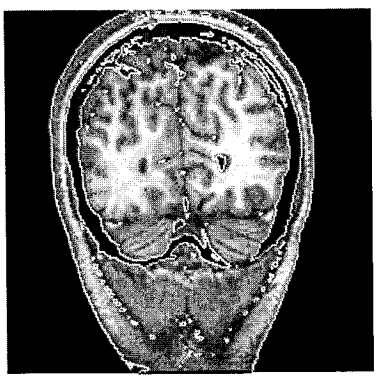

(c) Segmentation result for the first stage in [2].

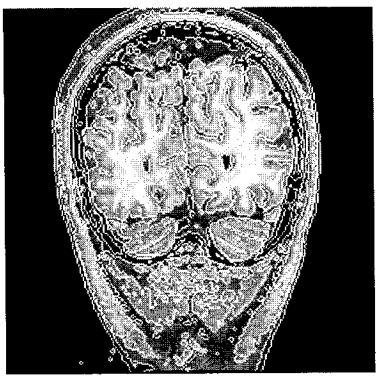

(d) Segmentation result for the second stage in [2]

(e) Segmentation result using our hierarchical segmentation scheme before merging regions and deleting noise regions.

(f) Final segmentation result using the new hierarchical segmentation scheme.

Figure 19: *Segmentation result of brain. Minimum scale:* 21×21*; minimum object contrast:* 10

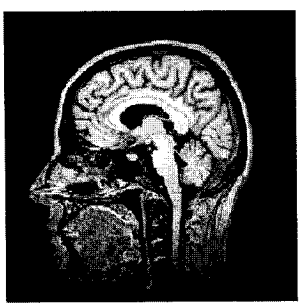

(a) Original image.

(b) Gaussian smoothed image.

(c) Segmentation result using Chan-Vese's approach in [4].

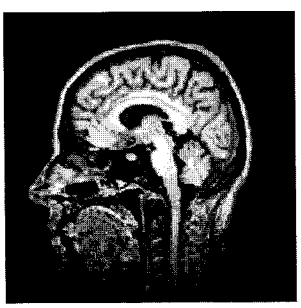

(d) Denoise result using Chan-Vese's approach in [4].

(e) Segmentation result using hierarchical segmentation approach in [2].

(f) Denoise result using the hierarchical segmentation approach in [2].

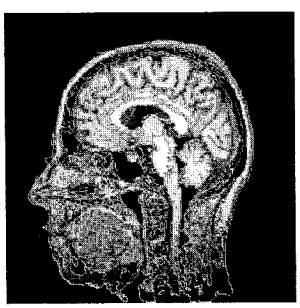

(g) Segmentation result using our hierarchical segmentation scheme.

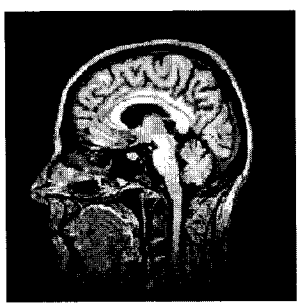

(h) Denoise result using our hierarchical segmentation scheme.

Figure 20: *Denoise result of head. Minimum scale:* 7×7*; minimum object contrast:* 10

(a) Original image.

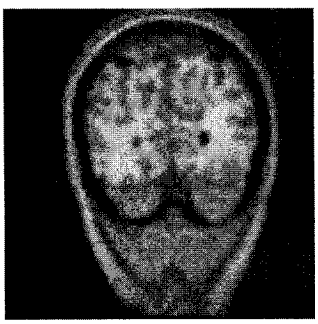

(b) Gaussian smoothed image.

(c) Segmentation result using Chan-Vese's approach in [4].

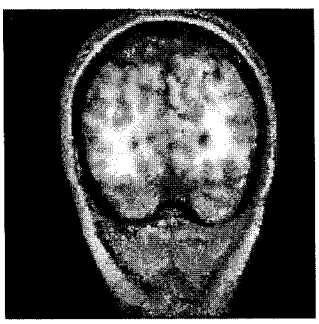

(d) Denoise result using Chan-Vese's approach in [4].

(e) Segmentation result using hierarchical segmentation approach in [2].

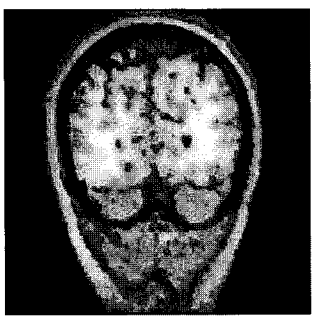

(f) Denoise result using the hierarchical segmentation approach in [2].

(g) Segmentation result using our hierhierarchical segmentation scheme.

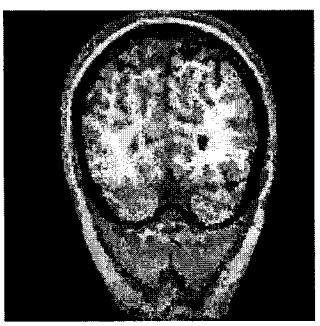

(h) Denoise result using our hierarchical segmentation scheme.

Figure 21: *Denoise result of brain. Minimum scale:* 11×11*; minimum object contrast:* 10

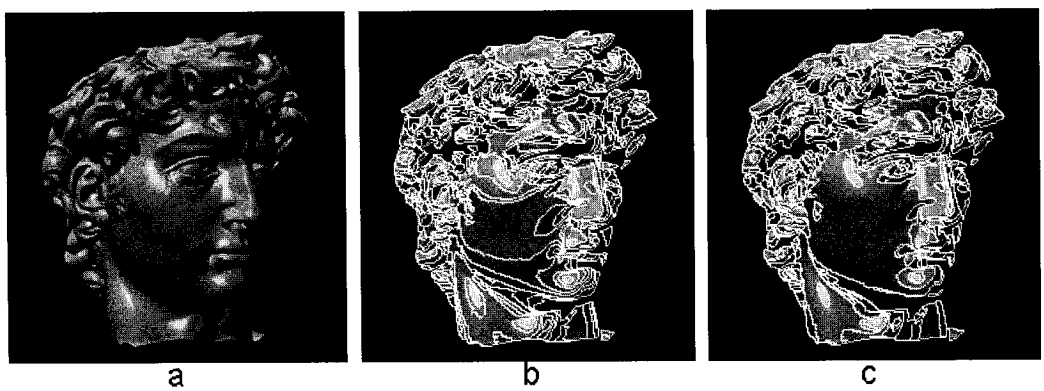

Figure 22: *Segmentation result of the head of David. (a) Original image; (b) Segmentation result using piecewise constant approximation and our hierarchical method; (c) Segmentation result using piecewise linear approximation and our hierarchical method.*

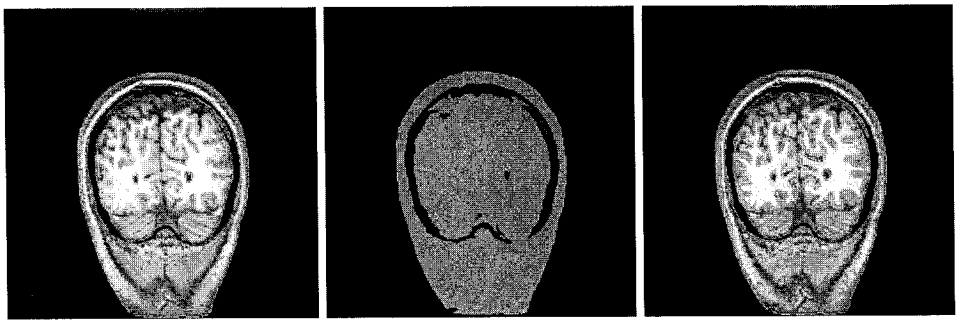

(a) Segmentation result. $T_a = 101 \times 101$.

(b) Reconstruction result. $T_a = 101 \times 101$.

(c) Segmentation result. $T_a = 41 \times 41$.

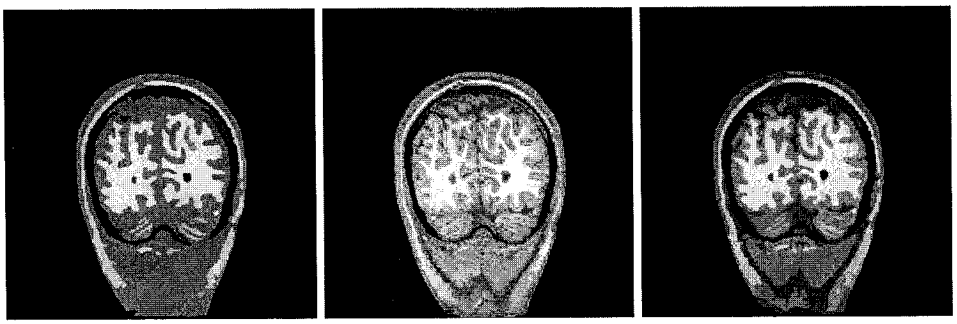

(d) Reconstruction result. $T_a = 41 \times 41$.

(e) Segmentation result. $T_a = 21 \times 21$.

(f) Reconstruction result. $T_a = 21 \times 21$.

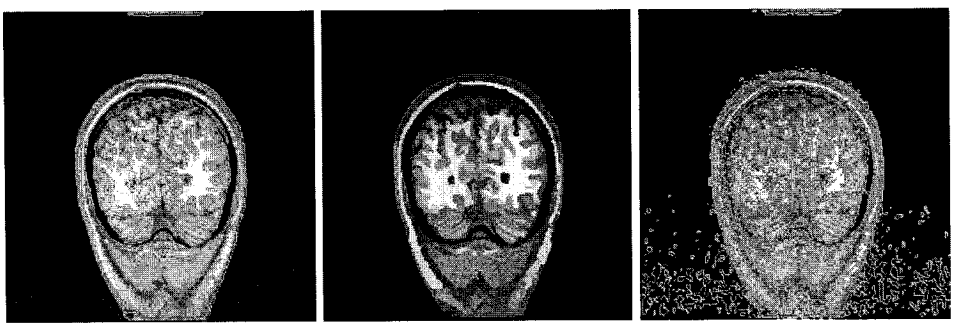

(g) Segmentation result. $T_a = 11 \times 11$.

(h) Reconstruction result. $T_a = 11 \times 11$.

(i) Segmentation result. $T_a = 5 \times 5$.

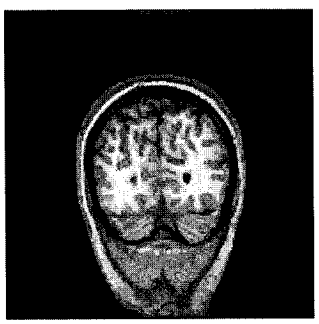

(j) Reconstruction result. $T_a = 5 \times 5$.

Figure 23: *Segmentation with different scale on brain.*

Chapter 7

Image Inpainting Using Hierarchical Level Set Approach

Image inpainting is originally an artistic procedure to recover a damaged painting or picture. It has been introduced in [31] and received attention from many researchers in computer vision and image processing. From a technical point of view, digital image inpainting can be described as a procedure to fill a defined *inpainting domain* (i.e. a set of damaged pixels in a given image). In this chapter, we propose a image inpainting approach based on the hierarchical Mumford-Shah model. Compared with previous works, my approach makes use of multi level set functions to detect and preserve the edges for both main structures and details.

7.1 Mumford-Shah Model for Inpainting

Tsai, Yezzi, and Willsky [1], and Chan and Shen [32] first presented the idea of applying the MS model to inpainting. For inpainting, they modified the MS model as:

$$\begin{aligned} E(u,C) &= \int_{\Omega} \lambda(x,y)\,|u-u_0|^2\,dxdy \\ &+ \mu \int_{\Omega\setminus C} |\nabla u|^2\,dxdy + \nu\cdot|C| \end{aligned} \tag{109}$$

where $\lambda(x,y) = 0$ if (x,y) is inside the inpainting area and 1 otherwise. The above equation indicates that only the variance of the image and the length of the segmentation curve are considered inside the inpainting area.

The solution of the MS energy functional is not a trivial task. There are some alternative solutions to this problem, such as piecewise smooth approximation of the Mumford-Shah model presented by Chan and Vese [4].

If we consider that a closed curve segments an image into two regions (i.e. both inside and outside regions), the MS energy functional can be written as:

$$\begin{aligned} E(u_1,u_2,C) &= \int_{\text{inside } C} \lambda(x,y)\,|u_1-u_0|^2\,dxdy + \mu\int_{\text{inside } C}|\nabla u_1|^2\,dxdy \\ &+ \int_{\text{outside } C}\lambda(x,y)\,|u_1-u_0|^2\,dxdy + \mu\int_{\text{outside } C}|\nabla u_2|^2\,dxdy + \nu\cdot|C| \end{aligned} \quad (110)$$

where u_1 and u_2 are smooth approximations of the image inside and outside the curve. The numerical solution of the MS energy functional can be implemented by the level set method. In the case that the image consists of two regions, the segmentation curve can be represented by one level set function ϕ:

$$\phi(x,y,t) = \begin{cases} > 0 & \text{if } (x,y) \text{ is inside } C \\ = 0 & \text{if } (x,y) \text{ is on } C \\ < 0 & \text{if } (x,y) \text{ is outside } C \end{cases} \quad (111)$$

Minimizing the functional $E(u_1,u_2,\phi)$ with respect to u_1, u_2, and ϕ, we obtain the equations for u_1, u_2, and ϕ as the following [5]:

$$\lambda(x,y)(u_1-u_0) = \mu\nabla^2 u_1 \text{ inside } C$$

$$\frac{\partial u_1}{\partial \vec{n}} = 0 \text{ on } C, \quad (112)$$

$$\lambda(x,y)(u_2-u_0) = \mu\nabla^2 u_2 \text{ outside } C$$

$$\frac{\partial u_2}{\partial \vec{n}} = 0 \text{ on } C, \quad (113)$$

$$\begin{aligned} \frac{\partial\phi}{\partial t} &= \delta(\phi)\Big[\nu\nabla\cdot\left(\frac{\nabla\phi}{|\nabla\phi|}\right) - \lambda(x,y)(u_1-u_0)^2 \\ &- \mu|\nabla u_1|^2 + \lambda(x,y)(u_2-u_0)^2 + \mu|\nabla u_2|^2\Big] \end{aligned} \quad (114)$$

The smooth image functions u_1 and u_2 can be obtained by solving the damped Poisson equations (112) and (113), and the segmentation curve can evolve according to equation (114).

This is the piecewise smooth approximation presented by Chan and Vese. Many advantages can be achieved by this approach, such as simultaneous segmentation and smoothing of noisy images, and detection of triple junctions by using multiple level set functions. However, because three PDEs equations (112), (113), and (112) needed to be solved simultaneously, the computational cost of this approach is very large. To overcome this difficulty, Chan and Vese proposed another approximation approach using the piecewise constant approximation [4, 5]. If the image intensities inside different regions are uniform, the image intensities inside different regions can be approximated by constants. In this case, the MS energy functional can be simplified to equation (115):

$$E(c_k, C) = \sum_k \int_{\Omega_k} \lambda(x,y)(c_k - u_0)^2 dxdy + \nu|C|, \tag{115}$$

where Ω_k represents the area inside each region. The gradient term in the MS energy functional disappears in equation (115) because the gradient inside each region is zero. Using the level set method [9] and the MS energy functional of the two phase segmentation, the image is segmented into two regions:

$$\begin{aligned} E(c_1, c_2, \phi) &= \int \lambda(x,y)(c_1 - u_0)^2 H(\phi) dxdy \\ &+ \int \lambda(x,y)(c_2 - u_0)^2 (1 - H(\phi)) dxdy \\ &+ \nu \int \delta(\phi)|\nabla\phi| dxdy \end{aligned} \tag{116}$$

where $H(x)$ is the Heaviside function. To minimize the energy functional with respect to c_1, c_2, and ϕ, we obtain the following equations:

$$c_1(\phi) = \frac{\int \lambda(x,y) u_0 H(\phi) dxdy}{\int H(\phi) dxdy} \tag{117}$$

$$c_2(\phi) = \frac{\int \lambda(x,y) u_0 (1 - H(\phi)) dxdy}{\int (1 - H(\phi)) dxdy} \tag{118}$$

$$\begin{aligned} \frac{\partial\phi}{\partial t} &= \delta(\phi)\Big[\nu\nabla \cdot \left(\frac{\nabla\phi}{|\nabla\phi|}\right) \\ &- \lambda(x,y)(u_0 - c_1)^2 + \lambda(x,y)(u_0 - c_2)^2\Big] \end{aligned} \tag{119}$$

After solving these equations, we can obtain the information on c_1, c_2, and C. The image u_0 will then be segmented into two regions $\{u = c_1\}$ and $\{u = c_2\}$, and the inpainting area will be filled.

7.2 Image Inpainting Based on Hierarchical Segmentation

In [2], Gao and Bui proposed a hierarchical method for image segmentation and smoothing based on the Mumford-Shah variational approach and the level set method. The method is fast and robust to the initial condition since the decoupled curve evolution PDEs are adopted.

Following their idea, we decouple the segmentation and diffusion in the process of image inpainting. To inpaint an image, we first segment the image using hierarchical segmentation scheme presented in this thesis, and determine the object boundaries inside the inpainting area. Then we use the diffusion technique to fill the inpainting area. To preserve the object boundary, the diffusion is only conducted from inside the object regions towards the inpainting area but not across the boundaries of the objects. Compared with previous works, my approach makes use of multi level set functions to detect and preserve the edges for both main structures and details.

Based on the hierarchical segmentation algorithm, the algorithm for image inpainting can be presented as follows. (For the sake of completeness, here we repeat the hierarchical algorithm for segmentation already presented in chapter 5. Therefore the difference between the algorithm given here and the one in chapter 5 is only in step 9 for inpainting.)

1. Define an initial closed curve. The area inside the curve corresponds to the area threshold T_a.

2. Move the initial curve to different positions in one region (in the beginning, the region is the whole image), and calculate the average intensities inside the curve and the whole region. If at any position, the absolute difference between the two average intensities is smaller than the contrast threshold T_c, the region needs no more segmentation. Otherwise, position the initial curve at the location where the absolute difference is the largest.

3. In the region (in the beginning, the region is the whole image), use piecewise constant approximation of the MS model to solve the curve evolution and obtain the segmentation result.

4. Number the different regions in the image.

5. In each region, repeat steps 2 and 3 to segment the region into smaller regions. In this step, all the calculations are inside one region.

6. Repeat 5 for each region obtained from different segmentation stages until all regions need no more segmentation.

7. Calculate the average intensity of each region. If the absolute difference between the average intensities of two neighbor regions is smaller than the contrast threshold used in step 2, T_c, the two regions are merged into one region.

8. Calculate the area of each region. If the area is too small, for example less than 10 pixels, the region is regarded as noise, and is merged into its neighboring region.

9. Use diffusing technique to fill the inpainting area. The diffusion is only conducted from inside the object regions towards the inpainting area but not across the boundaries of the objects.

7.3 Experimental Results

To show the advantage of our hierarchical segmentation and inpainting approach, we implement the inpainting algorithm using the total variance (TV) approach, the MS model approach with one level set function, and the MS model approach with hierarchical multi level set functions respectively.

Figure 24 is the inpainting results on the image of peppers. For the MS model approach, after segmentation of the image, we can detect the boundaries of objects in the inpainting area, and the edges of objects are kept very well. In the detail image (f) and (c), it is obvious that the inpainting result of MS model approach is better than that of TV approach.

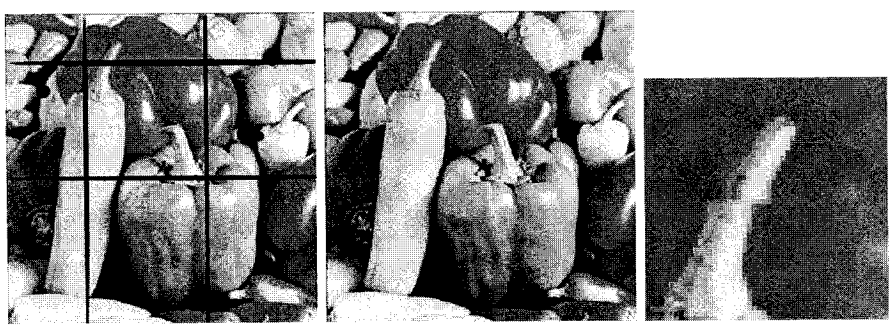

(a) image with inpainting lines (b) inpainting result with TV (c) detail of (b)

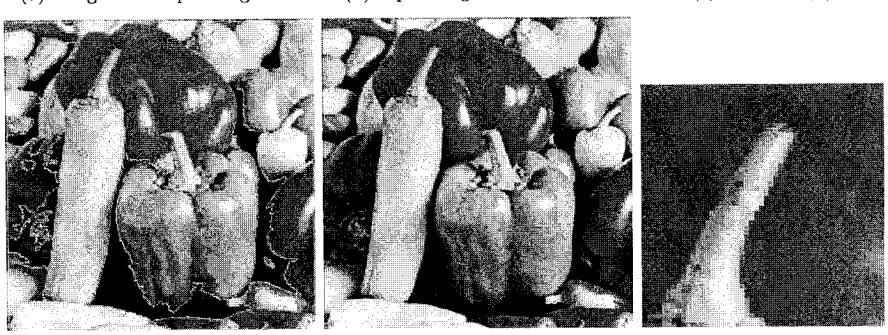

(d) segmentation result with MS (e) inpainting result with MS (f) detail of (e)

Figure 24: *The inpainting results on the image of peppers.*

Figure 25 shows the inpainting results on an artificial image. In addition of the TV approach and MS model approach of hierarchical multi level set functions, we also show the inpainting result with MS model approach of one level set function. Because one level set function cannot detect all the boundaries, many edges are blurred in the inpainting area. Our hierarchical segment and inpainting approach can detect all the boundaries, and keep all the edges clear in the inpainting result.

Figure 26 is the inpainting results on the image of a copy machine. Compared with result of one level set function, the inpainting result of hierarchical multi level set functions is much better. It can preserve the edges of the paper on the table clear.

Figure 27 is the inpainting results on the image of a street scene. Because the segmentation with hierarchical multi level set functions can detect more edges than the segmentation with only one level set function, more edges inside inpainting area can be preserved. While the edge of the car is blurred in the detail images (c) and (f), the edge is preserved in the detail image (i).

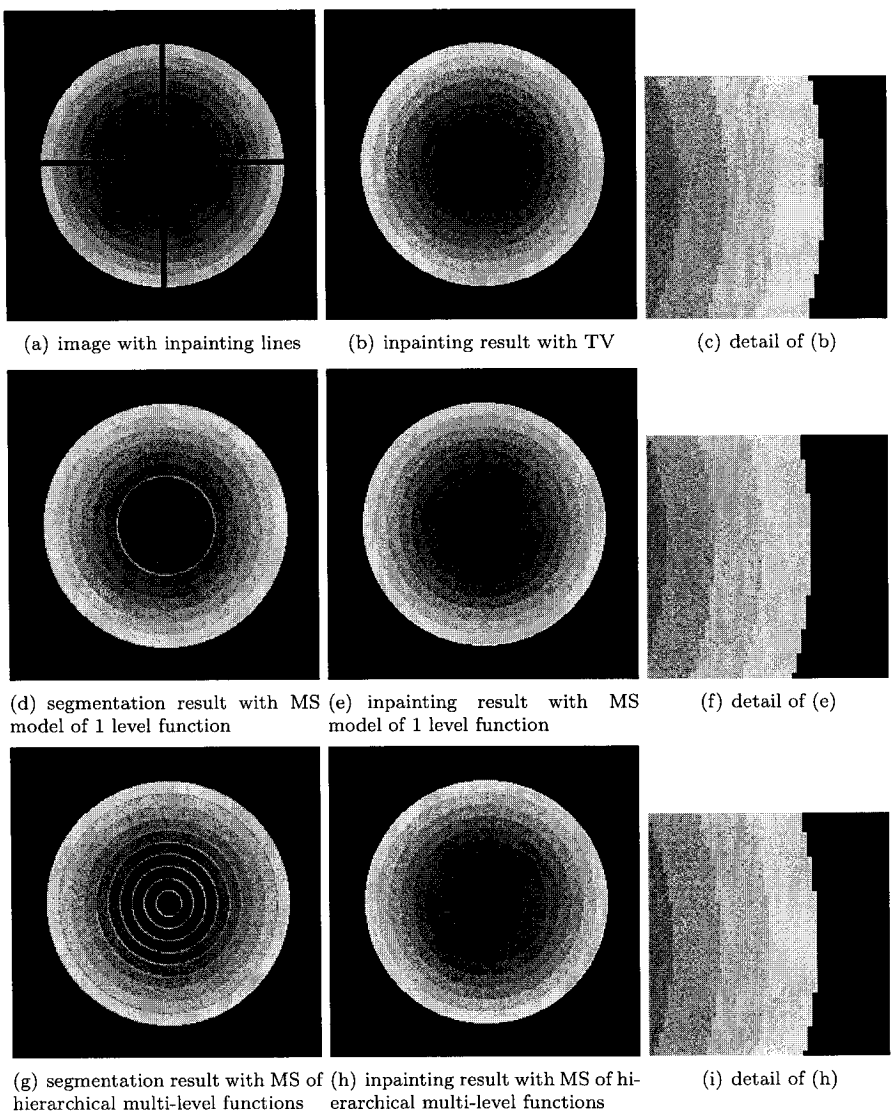

(a) image with inpainting lines (b) inpainting result with TV (c) detail of (b)

(d) segmentation result with MS model of 1 level function (e) inpainting result with MS model of 1 level function (f) detail of (e)

(g) segmentation result with MS of hierarchical multi-level functions (h) inpainting result with MS of hierarchical multi-level functions (i) detail of (h)

Figure 25: *The inpainting results of an artificial image.*

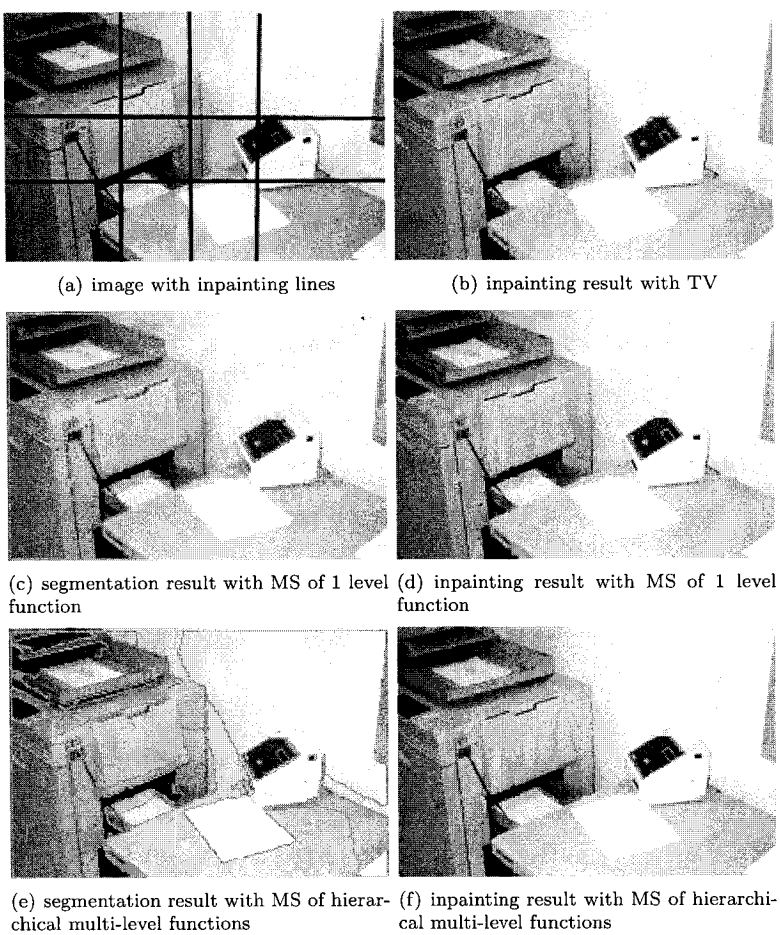

(a) image with inpainting lines

(b) inpainting result with TV

(c) segmentation result with MS of 1 level function

(d) inpainting result with MS of 1 level function

(e) segmentation result with MS of hierarchical multi-level functions

(f) inpainting result with MS of hierarchical multi-level functions

Figure 26: *The inpainting results on the image of a copy machine.*

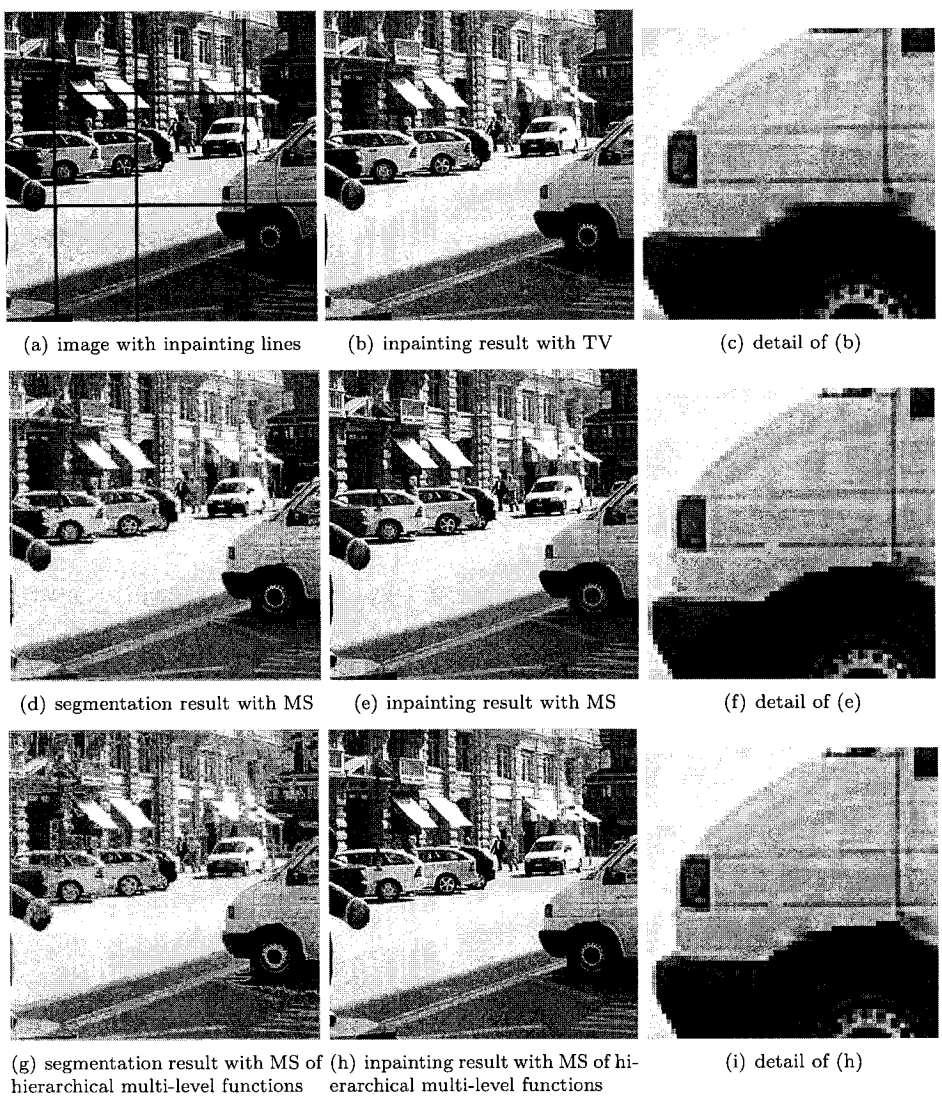

(a) image with inpainting lines (b) inpainting result with TV (c) detail of (b)

(d) segmentation result with MS (e) inpainting result with MS (f) detail of (e)

(g) segmentation result with MS of hierarchical multi-level functions (h) inpainting result with MS of hierarchical multi-level functions (i) detail of (h)

Figure 27: *The inpainting results on the image of euroexpress.*

Chapter 8

Conclusion

In this thesis, we have studied the Mumford-Shah model in some details and implemented it to solve image segmentation and image inpainting problems. We studied various approximations to the model including piecewise smooth, piecewise constant, and piecewise linear approximations. However, the original MS model has some drawbacks, such as its difficulty in the detection of roof edges. To overcome this difficulty, we investigated different variances of the MS model and propose to use second order derivative term to detect roof edges. We use piecewise linear approximation and level set functions to implement the modified MS model for this problem. The experimental results indicate that our method is effective.

The most important problem for MS model is the initial condition problem. Because the MS energy functional is not convex, the segmentation result is often trapped by the local minimum and cannot segment image correctly. We present a hierarchical segmentation scheme to overcome this problem. With this hierarchical segmentation scheme, we can segment an image into regions until each region is smooth enough and need no additional segmentation, that is, the final segmentation. Compared with previous works, our approach can automatically detect both the main structure and details in an image with multi level set functions, and it can automatically stop when all boundaries are detected. The final segmentation does not depend on the initial condition. In addition, the

solution of multi level set functions are decoupled, and the approach is also relatively fast and robust. Many results indicate that our approach is effective in many applications.

The MS model can also be used in image inpainting. Compared with other image inpainting approaches, the approach based on the MS model detect boundaries of objects and preserve edges in an image. We apply the new hierarchical segmentation scheme to image inpainting. Because our approach can detect both main structure and details edges in an image with multi level set functions, the new approach can preserve more edges and details compared with previous work.

Appendix A

Algorithm for Labeling Regions

Loop from the first row to the last row

Loop from the first column to the last column

If the current pixel is at the 1st row and 1st column

Create a new region number and the current pixel is assigned the region number;

Else if the current pixel is at the 1st row

If according to the segmentation result, the current pixel belongs to the same region as the pixel at the previous column and the same row

The current pixel is assigned the region number of the pixel at the previous column;

Else

Create a new region number and the current pixel is assigned the region number;

Else if the current pixel is at the 1st column

If according to the segmentation result, the current pixel belongs to the same region as the pixel at the previous row and the same column

The current pixel is assigned the region number of the pixel at the previous row;

Else

Create a new region number and the current pixel is assigned the region number;

Else if according to the segmentation result, the current pixel belongs to the

same region as the pixel at the previous column and the same row

The current pixel is assigned the region number of the pixel at the previous column;

If according to the segmentation result, the current pixel belongs to the same

region as the pixel at the previous row and the same column

All the pixels assigned as the region number of pixel at the previous row

are assigned as the region number of the current pixel;

Else if according to the segmentation result, the current pixel belongs to the same region

as the pixel at the previous row and the same column

The current pixel is assigned the region number of the pixel at the previous row;

Else

Create a new region number and the current pixel is assigned the region number;

End of loop for column

End of loop for row

Bibliography

[1] A. Tsai, A. Yezzi, and Alan S. Willsky, "Curve evolution implementation of the Mumford-Shah functionalal for image segmentation, denoising, dnterpolation, and magnification," IEEE Trans. on Image Processing, vol. 10, no. 8, pp.1169-1186, 2001.

[2] S. Gao and T. D. Bui, "Image segmentation and selective smoothing by using Mumford-Shah model," IEEE Trans on Image Processing, vol. 14, no. 10, pp.1537-1549, 2005.

[3] D. Mumford, and J. Shah, "Optimal approximation by piecewise smooth functionals and associated variational problems," Comm. Pure Appl. Math, Vol. 42, pp.577-685, 1989.

[4] T. F. Chan and L. A. Vese, "Active contours without edges," IEEE Trans on Image Processing, vol. 10, no. 2, pp.266-277, 2001.

[5] L. Vese and T. F. Chan, "A multiphase level set framework for image segmentation using the Mumford and Shah model," International Journal of Computer Vision, vol. 50, no. 3, pp.271-293, 2002.

[6] M. Kass, A. Witkin, and D. Terzopoulos, "Snake: Active contour models," International Journal of Computer Vision, vol. 1, pp.321-331, 1988.

[7] V. Casseles, R. Kimmel, and G. Sapiro, "Geodesic active contours," International Journal of Computer Vision, vol. 22, pp.61-79, 1997.

[8] A. Yezzi, L. Zollei, and T. Kapur, "A variational framework for integrating segmentation and registration through active contours," Medical Image Analysis, vol. 7, pp.171-185, 2003.

[9] J. A. Sethian, "Level set methods and fast marching methods," Cambridge University Press, 1999.

[10] G. Aubert and P. Kornprobst, "Mathematical problem in image processing: partial differential equations and the calculus of variations," Applied Mathematical Sciences, vol. 147, Springer, 2002.

[11] B. Song and T. F. Chan, "A fast algorithm for level set based optimization," UCLA CAM Report 02-68, December, 2002.

[12] S. Geman, and D. Geman, "Stochastic relaxation, Gibbs distribution, and the bayesian restoration of images," IEEE Trans. on PAMI, vol. 6, pp. 721-741, 1984.

[13] L. Rudin, S. Osher and E. Fatemi, "Nonlinear total variation based noise removal algorithms," Physica D, vol. 60, 259-268, 1992.

[14] L. A. Vese, "Multiphase object detection and image segmentation," Geometric Level Set Methods in Imaging, Vision and Graphics, S. Osher and N. Paragios (eds), Springer Verlag, pp. 175-194, 2003.

[15] R. A. Weisenseel, W.C. Karl, D.A. Castanon, "A region-based alternative for edge-preserving smoothing," Proceedings of the International Conference on Image Processing, pp. 778-781. Vancouver, BC, Canada, 2000.

[16] S. Gao and T. D. Bui, "A new image segmentation and smoothing model," Proceeding of IEEE International Symposium on Biomedical Imaging, pp. 137-140, April 15-18, 2004.

[17] J. Kim, J. W. Fisher, A. Yezzi, M. Cetin, and A. S. Willsky, "A nonparametric statistical method for image segmentation using information theory and curve evolution," IEEE Trans. on Image Processing, vol. 14, no. 10, pp.1486-1502, 2005

[18] V. Caselles, F. Catter, T. Col, and F. Dibos, "A geometric model for active contours in image processing," Numerische Mathematik, vol. 66, no. 1, pp. 1-31, 1993.

[19] G. Aubert, M. Barlaud, O. Faugeras, and S. Jehan-Besson, "Image segmentation using active contours: Calculus of variation or shape optimization?," SIAM J. Appl. Math., vol 63, no. 6, pp. 2128-2154, 2003.

[20] G. Aubert and P. Kornprobst, "Mathematical Problem in Image Processing: Partial Differential Equations and the Calculus of Variations," New York: Springer, vol. 147, 2002.

[21] T. D. Bui, S. Gao, and Q.H. Zhang, "A generalized Mumford-Shah model for roof-edge detection," IEEE International Conference on Image Processing, vol. 2, pp. 1214-1217, 2005.

[22] S. Osher and J. Sethian, "Fronts propagating with curvature-dependent speed : Algorithm based on the Hamilton-Jacobi formulation," Journal of Computational Physics, 79 pp12-49, 1988.

[23] S. Osher and N. Paragios, Geometric Level Set Methods, Springer, 2003.

[24] S. Osher and R. P. Fedkiw, "Level set Methods: An overview and some recent results," Journal of Computational Physics, vol. 169, pp.463-502, 2001.

[25] D. Adalsteinsson, and J. A. Sethian, "A Fast Level set methods for Propagating Interfaces," Journal of Computational Physics, vol. 118, no. 2, pp.269-277, 1995.

[26] H. K. Zhao, T. F. Chan, B. Merriman, S. Osher, "A Variational Level Set Approach to Multiphase Motion," Journal of Computational Physics, vol. 127, pp. 179-195, 1996.

[27] S. Osher and R. P. Fedkiw, Level set Methods and Dynamic Implicit Surfaces, Springer Verlag, 2002.

[28] H. K. Zhao, S. Osher, B. Merriman, and M. Kang,"Implicit and Nonparametric Shape Recognition from Unorganized Data Using a Variational Level set Method," Computer Vision and Image Understanding, vol. 80, pp. 295-314, 2000.

[29] Q. H. Zhang, "Mumford-Shah Model and its Application in Image Processing," Thesis for Master's Degree, Concordia University, 2005.

[30] S. Gao, "A New Segmentation and Smoothing Method Based on the Mumford-Shah Variational Model," Thesis for Master's Degree, Concordia University, 2003.

[31] M. Bertalmio, G. Sapiro, V. Caselles, and C. Ballester, "Image inpainting," ACM International Conference on Computer Graph- ics and Interactive Techniques (SIGGRAPH), pp. 417-424, 2000.

[32] T. F. Chan and J. Shen, "Mathematical models for local non-texture inpainting," SIAM J. Appl. Math., Vol. 62, no. 3, pp. 1019-1043, 2002.

[33] D. Terzopoulos, "Deformable models: classic, topology-adaptive and generalized formulations," in Geometric Level Set Method in Imaging, Vision, and Graphics, pp.21-40, edited by S. Osher and N. Paragios, Springer, 2003.

[34] S. Kichenassamy, A. Kumar, P. Olver, A. Tannenbaum, and A. Yezzi, "Gradient flows and geometric active contour models," International Conference on Computer Vision, pp. 810-815, June, 1995.

[35] G. Aubert, and L. Blanc Feraud, "Some remarks on the equivalence between classical snakes and geodesic active contours," International Journal of Computer Vision, vol. 34, no. 1, pp. 19-28, 1999.

[36] L. Ambrosio and V. M. Tortorelli, "Approximation of functionals depending on jumps by elliptic functionals via Γ-convergence," Comm. Pure Appl. Math., Vol. 43, pp. 999-1036, 1990.

[37] L. Ambrosio and V. M. Tortorelli, "On the approximation of free discontinuity problems," Boll. Un. Mat. Ital. B, Vol.7, No. 6, pp. 105-123, 1992.

[38] L. Ambrosio, L. Faina,and R. March, "Variational approximation of a second order free discontinuity problem in computer vision," SIAM J. MATH. ANAL., Vol. 32, No. 6, pp. 1171-1197, 2001.

[39] V. Caselles, R. Kimmel, and G. Sapiro, "Geodesic active contours," Proceedings of the 5-th International Conference on Computer Vision, pp. 694-699, MA, June 1995, IEEE Computer Society Press.

[40] S. Kichenassamy, A. Kumar, P. Olver, A. Tannenbaum, and A. Yezzi, "Conformal curvature flows: from phase transition to active vision," Archive for Rational Mechanics and analysis, Vol.134, pp. 275-301, 1996.

[41] P. Charbonnier, L. Blanc-Feraud, G. Aubert, and M. Barlaud, "Deterministic edge-preserving regularization in computer imaging," IEEE Trans. Image Process., Vol. 6, pp. 298-311, 1997.

[42] M. Kass, A. Witkin, and D. Terzopoulos, snake, Active Contour Models, "The International Journal of Computer Vision," Vol. 1, pp. 321-331, 1988.

[43] B. R. Lee, A. Ben Hamza and H. Krim, "An active contour model for image segmentation: a variational perspective," Proc. IEEE international conference on acoustics speech and Signal Processing, Orlando, May 2002.

[44] S. Z. Li, "Roof-Edge Preserving Image Smoothing Based on MRFs," IEEE Transactions On Image Processing, Vol. 9, No. 6, pp.1134-1138, June 2000.

[45] S. Teboul, L. Blanc-Feraud, G. Aubert, and M. Barlaud, "Variational Approach for Edge-Preserving Regularization Using Coupled PDEs," IEEE Transactions On Image Processing, Vol. 7, No. 3, pp. 387-397, March 1998.

[46] A. Yezzi, A. Tsai, and A. Willsky, "A statistical approach to snakes for bimodal and trimodal imagery," Proc. Int. Conf. Computer Vision, 1999.

[47] T. Chan, J. Shen, and L. Vese, "Variational PDE Models in Image Processing," Notices of the American Mathematical Society, vol. 50, no. 1, pp. 14-26, Jan. 2003.

[48] T. F. Chan, B. Y. Sandberg, and L. A. Vese, "Active Contours without Edges for Vector-Valued Images," Journal of Visual Communication and Image Representation vol 11, pp.130-141, 2000.

[49] J. Weickert, Anisotropic diffusion in Image Processing, Teubner, Stuttgart (1998).

[50] S.Z. Li, Markov Random Field Modeling in Image Analysis, Springer, 2001.

[51] A. Blake and A. Zisserman, Visual Reconstruction, The MIT Press, Cambridge, Massachusetts, 1987.

[52] S. Osher and N. Paragios, Geometric Level Set Methods, Springer, 2003.

[53] W. Vanzella, F.A. Pellegrino, and V. Torre, "Self-Adaptive Regularization," IEEE Transactions On PAMI, Vol. 26, No. 6, pp. 804-809, June 2004.

[54] E. Y. Kim, S. H. Park, and H. J. Kim, "A Genetic Algorithm-Based-Segmentation of Markov Random Field Modeled Images," IEEE Signal Processing Letters, vol 7, no 11, pp.301-303, 2000.

[55] A. Sarkar, M. K. Biswas, and K. M. S. Shama, " A simple Unsupervised MRF Model Based Image Segmentation Approach," IEEE Transactions on Image Processing, vol. 9, no. 5, pp.801-812, 2000.

[56] R. Wilson and M. Spann, Image segmentation and Uncertainty, John Wiley & Sons Inc. 1988.

[57] J. C. Russ, the Image Processing Handbook, CRC press, Inc, 1992.